EXPERIMENTAL ANALYSIS OF THE EFFECT OF CARTILAGINOUS RINGS IN TRACHEOBRONCHIAL FLOW AND STENOTIC TRACHEA FLOW

by

**Jose Alberto Montoya Segnini**

A Thesis

Submitted to the Faculty of Purdue University

In Partial Fulfillment of the Requirements for the degree of

Master of Science in Mechanical Engineering
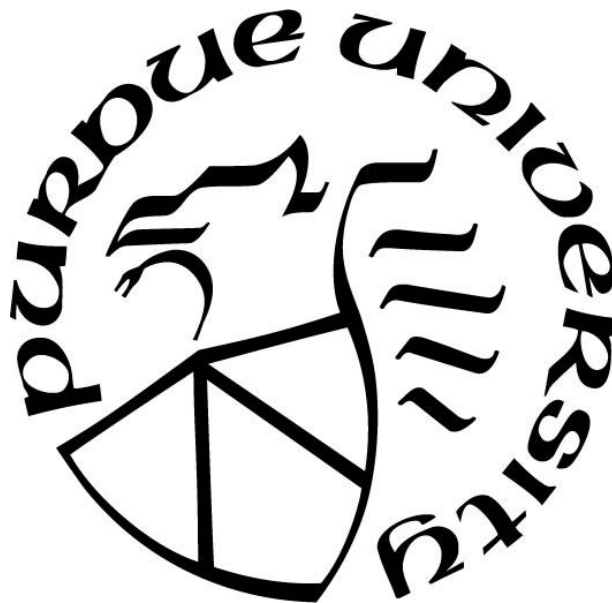
School of Mechanical Engineering

West Lafayette, Indiana

August 2019

THE PURDUE UNIVERSITY GRADUATE SCHOOL
STATEMENT OF COMMITTEE APPROVAL

Dr. Luciano Castillo, Chair

    School of Mechanical Engineering

Dr. Jun Chen

    School of Mechanical Engineering

Dr. Steve Wereley

    School of Mechanical Engineering

Approved by:

    Dr. Jay Gore

        Head of the Graduate Program

Dedication

This study is dedicated to my beloved parents, who by example of hard work and persistence have taught me that there is no limit to what one can accomplish. To my brother, for being an inspiration of working towards your dreams. And lastly, to my beloved girlfriend, whom support in the last years have been crucial to keep moving forward under difficult moments during this work.

ACKNOWLEDGMENTS

TABLE OF CONTENTS

LIST OF TABLES

LIST OF FIGURES

ABSTRACT

Author: Montoya Segnini, Jose, A. MS
Institution: Purdue University
Degree Received: August 2019
Title: Experimental Analysis of the Effect of Cartilaginous Rings in Tracheobronchial Flow and Stenotic Trachea Flow
Committee Chair: Luciano Castillo

An accurate understanding of the respiratory fluid dynamics is instrumental for medical applications, such as drug delivery system and treatment of diseases. Substantial research has been done to study such flow. However, a great number of these studies have the prevailing assumption of having a smooth wall, in despite the human trachea and bronchi is sustain by a series of cartilaginous rings, which creates height differences near the wall. To study the effect of including cartilaginous rings in the respiratory flow we developed two experiments, presenting a comparison between a smooth model and a model with cartilaginous rings. First, we present an experimental observation of a simplified Weibel-based model of the human trachea and bronchi with cartilaginous rings. The experiments were carried out with a flow rate comparable with a resting state (trachea-based Reynolds number of $Re_D = 2650$). In the second experiment, we developed a similar experiment but in a model with a tracheal stenosis (70% in the middle of the model) and no bronchi. In this case we increase the Reynolds number to $Re_D = 3350$, still a resting breathing state condition.

For both experiments, we used transparent models and refractive index-matching methods were used to observe the flow, particularly near the wall. The flow was seeded with tracers to perform particle image velocimetry and particle tracking velocimetry to quantify the effect the rings have on the flow near the trachea and bronchi walls. From the results, we present a previously unknown phenomenon in the cavities between the cartilaginous rings: a small recirculation is observed in the upstream side of the cavities throughout the trachea. This recirculation is due to the adverse pressure gradient created by the expansion, which traps particles within the ring cavity. In addition, we found that the cartilaginous rings induce velocity fluctuations into the flow, which enhances the near-wall momentum of the flow reducing the separation after the stenosis. Size of the recirculation is reduced by 11% and the maximum

upstream velocity is reduced by 38%, resulting in a much weaker recirculation because of the rings. Also noticed a delay in the separation from the trachea to bronchi bifurcation.

The detection of recirculation zones in the cartilage ring cavities and the perturbation sheds light on the particle deposition mechanism and helps explain results from previous studies that have observed an enhancement of particle deposition in models with cartilage rings. The results highlight the importance to include the cartilaginous rings in respiratory flow studies. Finally, we compared the results from the stenotic case with Reynolds-averaged Navier-Stokes (RANS) models ($k - \varepsilon$, $k - \varepsilon$ RNG, $k - \omega$, $k - \omega$ SST, $k - \omega$ SST LRN and 4-equation Transition SST). In the results, indicate significant discrepancies between the experimental measurements and the simulations, mainly in the area with flow separation after the contraction. Therefore, RANS algorithms should not be considered reliable for research purposes in respiratory fluid dynamics without experimental validation.

INTRODUCTION

It is important to have an accurate understanding of the airflow characteristics going through the respiratory system for different medical applications. Such applications include the study of particle deposition, which are studied for drug delivery (which research allows optimizing treatments) or for pollutants (to observe the adversary effects of contaminants in the environment). Along with the development of new, or analysis of old, diagnoses and treatment protocols for certain respiratory diseases. In order to have a good understanding of the flow behavior inside our airway ducts many studies have been developed for years and is a topic continuously being studied in the present.

The flow in the respiratory system is very complex and determining its characteristics theoretically is challenging due to several factors. From the beginning, the inlet geometry is complex and creates elaborated inlet conditions (Grgic, B., Finlay, W., Heenan, 2004). Followed by the flow being underdeveloped by the short distances (Schroter & Sudlow, 1969) and, the recurring bifurcation of the airways paths adds even more intricacy to the flow (Minnich & Mathisen, 2007). Diverse studies have studied the flow in the respiratory system; experimentally and by computer simulations, which we will review with more detail through this thesis. However, most of the studies previously done does not include the presence of ***cartilaginous rings***.

The trachea and bronchi are lined by a series of C-shaped cartilaginous rings and connected by a posterior membrane (Minnich & Mathisen, 2007). The rings serve as a structural component avoiding the pathways to collapse. These cartilaginous rings create differences in height through the wall which will alter the flow, this height differences have been measure by Russo, Robinson and Oldham (2008), also these height differences can also be appreciated in bronchoscopies. As previously mentioned, most studies done for tracheobronchial flow does not include the presence of the cartilaginous rings, assuming the walls as smooth. In this thesis we will review and study the effects of the cartilaginous rings have in the tracheobronchial flow.

Additionally, we evaluate the effect of the cartilaginous rings experimentally through Particle Image Velocimetry (PIV) in a refractive-index facility. The content is divided three main chapters: Chapter 1: Flow recirculation in cartilaginous ring cavities, where we study the effect of the rings near the wall with high-resolution observation in a tracheobronchial model. Chapter

2: Tracheal Stenosis with cartilaginous rings, we study the effects of the rings have on a disease that causes a contraction in the pathway, along with studying the fluid characteristics of the flow over the rings. Finally, in Chapter 3: Evaluation of RANS CFD in the study of respiratory flow, we compared our experimental results with one of the most used tools used to model the respiratory systems, the Reynolds Average Navier-Stokes (RANS) computational fluid dynamics (CFD). Each chapter including an individual literature review, description of the methodology used and discussion of results.

CHAPTER 1: FLOW RECIRCULATION IN CARTILAGINOUS RINGS CAVITIES

1.1 Introduction and literature review

As previously mentioned in the introduction, many studies have been done to research the tracheobronchial flow, yet, most of them have make the simplification of considering the wall surface as smooth. The cartilaginous rings are present inside the trachea and the top generations of the bronchi. To know the exact measurements of the rings, in a study made by Russo et al. (2008), they measured a whole lung specimen from a cadaver. The measured depth of the rings were 0.254 mm in an 18 mm diameter trachea. Other measurements can be found in Table 1.

Table 1: Cartilaginous rings measurements (Russo et al., 2008).

Measurements	Average (mm)
Width	3.21
Length between rings	2.98
Depth	0.254

Adler & Brücker (2007) studied the flow experimentally through PIV a realistic lung geometry from the trachea with six generations of branching. They did measurements at resting conditions and high frequency ventilation; however, the walls of the model were smooth. Similarly to Adler's study, other studies have make complex geometries for their trachea models for experimental PIV and computer simulated CFD studies assuming smooth walls for their models (Bauer & Brücker, 2015; Bauer, Rudert, & Brücker, 2012; Comer, Kleinstreuer, & Zhang, 2001b; Ramuzat & Riethmuller, 2002; Zhao & Lieber, 1994). Along with these studies of the flow characteristics, research of particle deposition have also been investigated on models assuming smooth walls (Belka, Lippay, Lizal, Jedelsky, & Jicha, 2014; Comer, Kleinstreuer, & Zhang, 2001a; Lizal, Jedelsky, Elcner, & Al., 2012; Mauder, T., Jedelsky, J. and Lizal, 2009).

More recently, realistic models have been studied from computer tomography (CT) scans. Nonetheless, CT scans have a limited resolution close to the height difference created by the cartilaginous rings and with the smoothing to build a 3D model the height differences are being smoothed (Freitas & Schröder, 2008; Grobe, Schröder, Klaas, Klöckner, & Roggenkamp, 2007; Kim & Chung, 2009; Luo & Liu, 2008; Pedley, Schroter, & Sudlow, 2006). For example,

in a CFD study from Luo & Liu (2008), based their model on CT scan measurements and observed the effect of the cartilaginous rings. Fluctuations were found in the flow near the wall induced by the rings, but, the flow disturbance was reported as ''not strong enough to cause a boundary layer separation''. However, from their figures, the rings appear to have a shallow depth (the authors did not provide the actual depth value). This shallow appearance could be due to the limited resolution of the CT scan of 0.7 mm, where the average ring depth found by Russo et al. (2008) was 0.25mm. Besides the resolution limitations, the CT scans are patient specific and shape vary between individuals, making it difficult to apply the results to the general population.

Only a few studies have incorporated the cartilaginous rings and examined the effect these give to the flow. As previously mentioned, Russo et al. (2008), who measured the cartilaginous rings, incorporated the rings in a CFD study. Comparing a smooth model and one with rings, found that an increment in particle deposition is found in the 'ringed' model. Also, demonstrated that the effect of the rings increases at higher flow rates and bigger particle sizes, for particle deposition. Similarly, in another CFD study by Srivastav, Paul, and Jain (2013), also investigated the effect of the cartilaginous rings. Srivastav et al. (2013) compared two models, a CT scan model with rings present versus a simplified model with a smooth wall. Little differences were found between cases, with slight increment of shear over the cartilaginous rings and increment in particle deposition. However, in this study there is a significant geometrical differences between models, which makes it difficult to compare both results. These two studies have been simulated on CFD however, it is important to validate the CFD results with high fidelity experiments.

In another study, Zhang and Finlay (2005) performed an experimental study on the effect of the cartilaginous rings in the particle deposition. Using two models, a smooth walled model and a cartilaginous rings model, it was found an enhanced deposition in the model with rings. However, the model used does not grant visual access and the flow characteristics remain unknown.

To study the flow characteristics Bocanegra Evans and Castillo (2016) presented PIV measurements in an index-matched model, such model is used for the purpose of this thesis and its characteristics are to be discussed in the methodology. Similarly, comparing a smooth model and a rough model demonstrated significant differences between models. The models included

the main trachea and bronchi, in which it was found a larger separation bubble at the bronchi entrance for the smooth model, which consequently affect the prediction of particle deposition. Furthermore, a higher vorticity is found along the trachea walls for the 'ringed' model, while higher vorticity is observed at the bottom of the bronchi for the smooth model. As stated by the authors, these differences could affect greatly the subsequently bronchi generations and hence the aerosol transport.

While these recent studies demonstrated the importance to consider the cartilaginous rings in tracheobronchial models (Bocanegra Evans & Castillo, 2016; Russo et al., 2008; Srivastav et al., 2013; Y. Zhang & Finlay, 2005), there is still much to learn from the effect of the cartilaginous rings have in the tracheobronchial flow. Thus, in this chapter it is studied the flow behavior near the wall with more detail. To help understand the particle deposition enhancement presented by Russo et al. (2008) and Zhang and Finlay (2005).

1.2 Methodology

Two simplified tracheobronchial models, a smooth walled model and a model with cartilaginous rings, were used to compared with 2D particle image velocimetry measurements (Adrian & Westerweel, 2011). The models consist of two generations, trachea and main bronchi, and it has a circular cross sectional area, its geometry is based on the study by Weibel (1963). The models were created by Bocanegra Evans and Castillo (2016). The typical diameter of the human trachea is 18 mm and for the bronchi is 12.2 mm (Maury, 2013). The models dimensions were scaled up by 67% to have a better resolution, with a trachea and bronchi diameter of 30 mm and 20.1 mm, respectively. The model with the cartilaginous rings have the rings dimensions also scaled up by a 67% from Russo et al. (2008), in Table 1. The new ring dimensions are 0.424 mm for the ring height, a width of 4.58 mm and a separation between rings of 5.76 mm. The models have a right bronchi angle of 25° and a left bronchi angle of 45°, resulting in a 70° intrabronchial angle, which according to Grotberg (1994) the intrabronchial angles rages from 64° to 100°. Model dimensions can be observed in Figure 1.
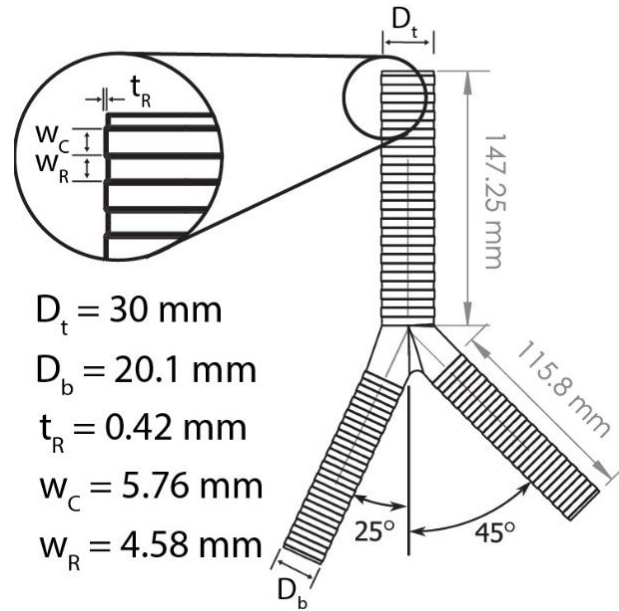
Figure 1: Trachea model dimensions.

The tracheobronchial models are made from polydimethylsiloxane (PDMS), a transparent silicone. This material has a refractive index number of 1.4, which it is matched with the working fluid to provide optical access to measure the flow inside (Shuib, Hoskins, Easson, & Model, 2010). And as working fluid it is used a liquid mixture of water, glycerin and salt with a mass percentage of 47.9%, 37.1% and 15% respectively. To be able to compare the results from the liquid working fluid to those of airflow inside the respiratory system the Reynolds number (Re) is matched. The Reynolds number is a scaling non-dimensional parameter; it is the ratio of the inertial forces and the viscous forces. Re for flow in a pipe is define in Equation (1).

$$\text{Re} = \frac{DU}{\upsilon} \qquad (1)$$

Where D is the pipe diameter, U the bulk (or average) velocity and υ the kinematic viscosity. With a trachea diameter $D_t = 30$ mm, a bulk velocity $U = 0.51$ m/s (flow rate of $Q = 21.6$ L/min) and a kinematic viscosity $\upsilon = 5.77 \times 10^{-6}$ m^2/s (density $\rho = 1080$ kg/m^3), Re = 2650, resembling resting breathing conditions (Z. Zhang, Kleinstreuer, & Kim, 2002).

For the fabrication of the models, by Bocanegra Evans and Castillo (2016), two single-piece, one for smooth-walled and one for the 'ringed' model, were 3D printed. A silicon robber mold was extracted from the 3D printed parts and glycerin soap boss were obtained. The soap boss was used as negative, where the PDMS is poured over the soap and after the PDMS is

cured, the model is submerged in hot water to dissolve the soap and obtain the trachea models. Because of the smooth finish of the surface and the index matched, evaluated by Bocanegra Evans and Castillo (2016), minimum reflections and distortions are created by the model, allowing detailed measurement even near the walls.

We only evaluate inspiratory flow for the purpose of this experiment. The flow is given at a constant rate and is driven by gravity. A schematic of the experimental setup can be observed in Figure 2. Two valves are adjusted to keep a steady level through the experiments, the level variation of both reservoir are less than 5%. The flow is supplied from the upper reservoir, and driven by gravity, supplied to the trachea model. The flow then is move from the tank to the lower reservoir, also by gravity, and finally the flow is returned to the upper reservoir with a pump. The length from the valve to the trachea model is 48 cm and the trachea length is 14.7 cm, total of 62.7 cm, this distance is not enough to have a fully developed flow. Since a length greater than 50 trachea diameters (150 cm) is needed to develop (Munson, Young, & Okiishi., 1990). Additionally, the epiglottis generates a jet in the entrance of the trachea (C. L. Lin, Tawhai, McLennan, & Hoffman, 2007). In case of the present experiments, even though it does not have the jet at the entrance or a developed flow, the inlet of the flow evaluated under equal circumstances, allowing a fair comparison.
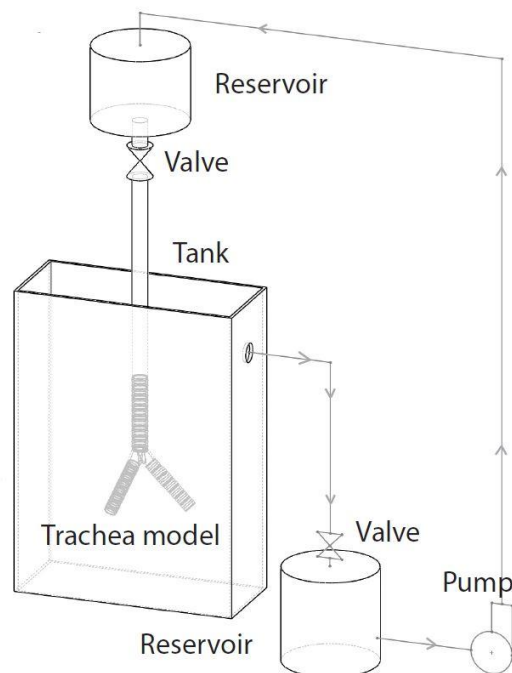

Figure 2: Experimental setup schematic.

1.2.1. PIV setup

The working fluid is seeded with polyamide fluorescent particles from Kanomax, NJ, the seeded particles are also known as tracer particles. The particles have a density $\rho_p = 1100$ kg/m^3 and a mean diameter $d_p = 15$ μm. To understand how the particles behave in the working fluid is needed to know how heavy the particles are in relation to the mean flow, which is the inertia of the suspended particles. It can be quantified by using the Stokes number (St), defined in Equation (2).

$$St = \frac{t_0 U}{l_0} \tag{2}$$

Where t_0 is the relaxation time, U is the bulk velocity of the fluid and l_0 is the characteristic dimension, for this case the particle diameter. The relaxation time is defined in Equation (3).

$$t_0 = \frac{\rho_d d_p^2}{18 \mu_f} \tag{3}$$

where p_d is the density difference between the particle density (1100 kg/m^3) and the fluid density (1080 kg/m^3), d_p is the particle diameter (15 μm), and μ_f is the fluid dynamic viscosity (6.23×10^{-3} N·s/m^2), resulting in $St = 0.00136$. For values less than 0.1 tracing accuracy errors are below 1%, and by being down to 10^{-3} are consider good passive tracers (Tropea, Yarin, & Foss, 2007).

A dual-head 532 nm Nd:YAG pulsed laser (Evergreen 145, Quantel) is used to illuminate the particles with a thin light sheet of approximately 1 mm. The laser illuminate the model from the side of the tank and to highlight the middle frontal plane of the model. Images were capture by a 14-bit CCD camera with a resolution of 1200×1600 pixels (ImagerProX; LaVision, Gottingen, Germany) with an 85 mm objective (Nikon Corp., Melville, NY) and a long-pass filter (OG 550, Edmund Optics).

As mentioned, Bocanegra Evans and Castillo (2016) observe the flow characteristics of the whole trachea model. However, the resolution used, of 21 pixels/mm, was not able to capture the flow characteristics near the wall. Hence, in this study two sets of data were taken to evaluate the models. A low-resolution set of data (LRD), with 36.7 pixels/mm, covering the entire trachea with 25 stations and a set of high-resolution data (HRD), with 64 pixels/mm, with 9 stations (3 along the trachea and 2 for each bronchi). 2000 images pairs were collected per station. The LRD set was processed with a multi-pass PIV algorithm (LaVision), with an initial interrogation

window of 96×96 pixel^2 and a final interrogation window of 32×32 pixel^2, with a 75% of overlap.

PIV determines the local flow velocities of particles in sub-regions of the image (Hart, 1998). However, since the depth of the rings (0.42 mm) is less than the side length of the final interrogation window of the LRD (32×32 pixel^2 = 0.87×0.87 mm^2) a HRD set was obtained and processed with Particle Tracking Velocimetry (PTV). The PTV analyzes each particle individual track and higher resolution velocity fields can be obtained near the wall, allowing observation of flow features difficult to observe with other methods (Thomas Janke, Schwarze, & Bauer, 2017; Maas, Gruen, & Papantoniou, 1993). The HRD set was processed with a hybrid PIV+PTV algorithm (LaVision), with an initial interrogation window of 96×96 pixel^2 and particle tracking for final step. Time separation between frames for both sets is adapted to limit the particles displacement to be less than 30 pixels.

1.3. Results and Discussion

Velocity contours and streamlines were obtained from the PIV analysis for both models, shown in Figure 3. The results show flow separation in the bifurcation at the upper wall of the bronchi, similarly as reported by Schroter and Sudlow (1969) and again by Pedley et al. (2006). As observed in the complete contours in Figure 3, and with more detail in Figure 4, Figure 4: Velocity contour at bifurcation for (A) smooth model and (B) 'ringed' model from PIV analysisthe separation is bigger and stronger for the smooth model than the model with cartilaginous rings. As previously reported by Bocanegra Evans and Castillo (2016).
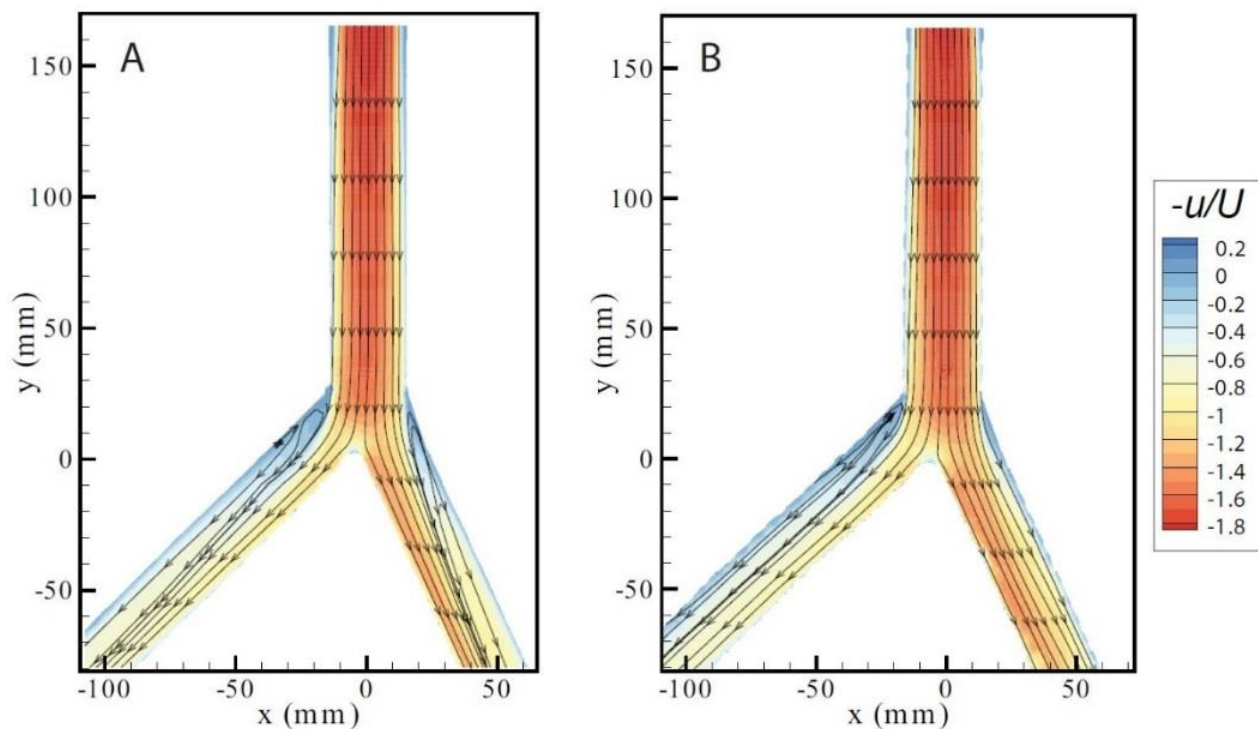
Figure 3: Velocity contour for (A) smooth model and (B) 'ringed' model from PIV analysis.
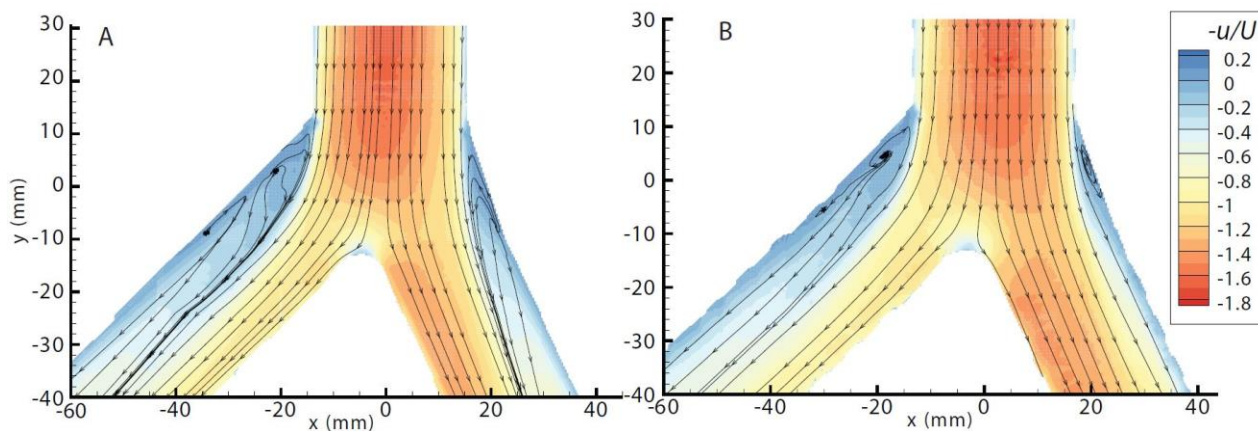
Figure 4: Velocity contour at bifurcation for (A) smooth model and (B) 'ringed' model from PIV analysis.

Velocity profiles, normal velocity fluctuations $[u'^2]$ and uv fluctuations from PIV analysis are shown in Figure 5. Similar velocity entry is observed in the top velocity profile, which means there is equal inlet conditions for both cases. However, at the middle and bottom profiles there is a slight inclination of the flow towards the right bronchi. No distinguishable differences can be observed from the left bronchi velocity profiles. On the other hand, the right bronchi present higher velocities on the top side of the bronchi for the ringed model, which occurs because of the smaller separation. Regarding the velocity fluctuations, both models present similar results at the trachea and bronchi, except at the bottom of the bronchi. Caused by the differences from the sizes of the separation regions, the smooth model present higher fluctuations at the bottom of the bronchi. As reported by Bocanegra Evans and Castillo (2016), such differences can affect the lower generations.
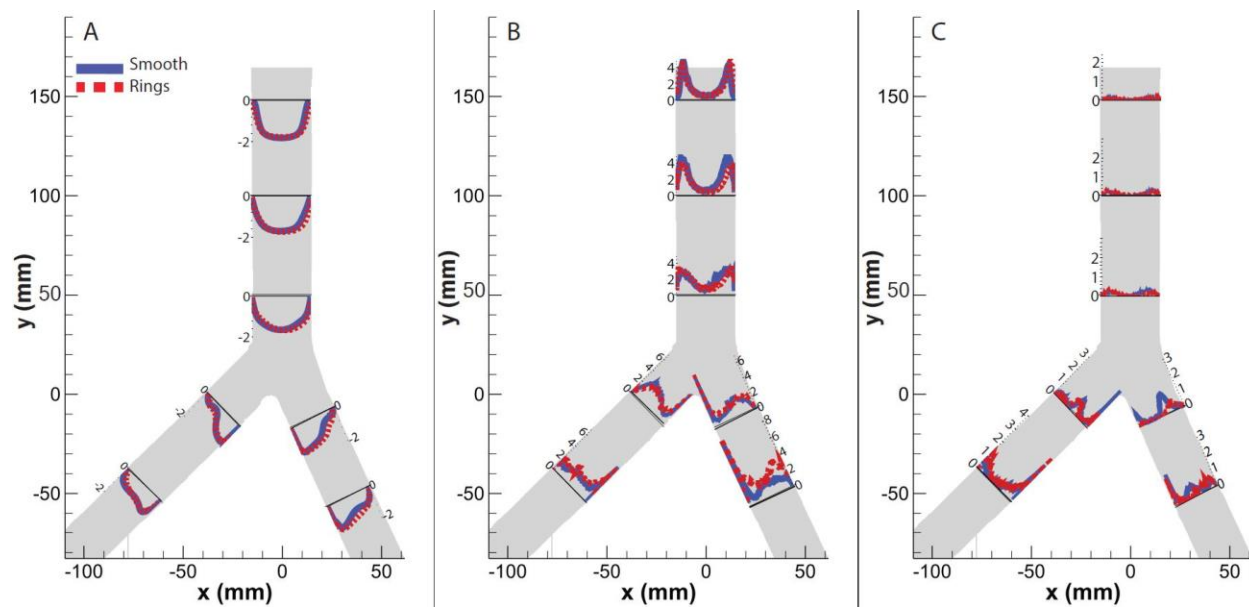
Figure 5 PIV analysis: (A) normalized velocity profiles $[u/U_{max}]$, (B) normal velocity fluctuations $[u'^2/U_{max}^2]$, and (C) uv fluctuations $[u'v'/U_{max}^2]$.

A phenomenon was observed from the images from the LRD set, where it was notice a particle displacement moving upstream at the cavities between rings. Such phenomenon was not captured by the PIV processing due to the low resolution and window size being bigger than the height difference between the rings, hence not being able to capture the displacement that close to the wall, as explained in Section 1.2.1. Though, by visual inspection particles were notice to be moving upstream at the cavities. A sample data image can be observed in Figure 6A, and 10

superimposed images in Figure 6B and 6C at the upstream side of the cavities between rings. The particle trajectory is noted to move upstream and when approaching the ring the particle moves away from the wall and then is recaptured by the incoming bulk flow.

Such particles are being trapped by a recirculation zone, created by the adverse pressure gradient at the expansion of the wall. Even though the data obtained is not time resolved, it was possible to recover particle trajectories near the wall due to the low velocity found in this area. This discovery is in contrast to Luo and Liu's (2008) study, where in a CT scan model they report that the effect of the rings were not strong enough to cause the recirculation. Unfortunately, the authors did not provide the depth of the rings, but, from their figures the rings appear to be too shallow, this possibly because of the limited resolution from the CT scan. Along with other previous studies that did not captured this phenomenon, including studies on the effect of cartilaginous rings on the flow (Bocanegra Evans & Castillo, 2016; Srivastav et al., 2013).
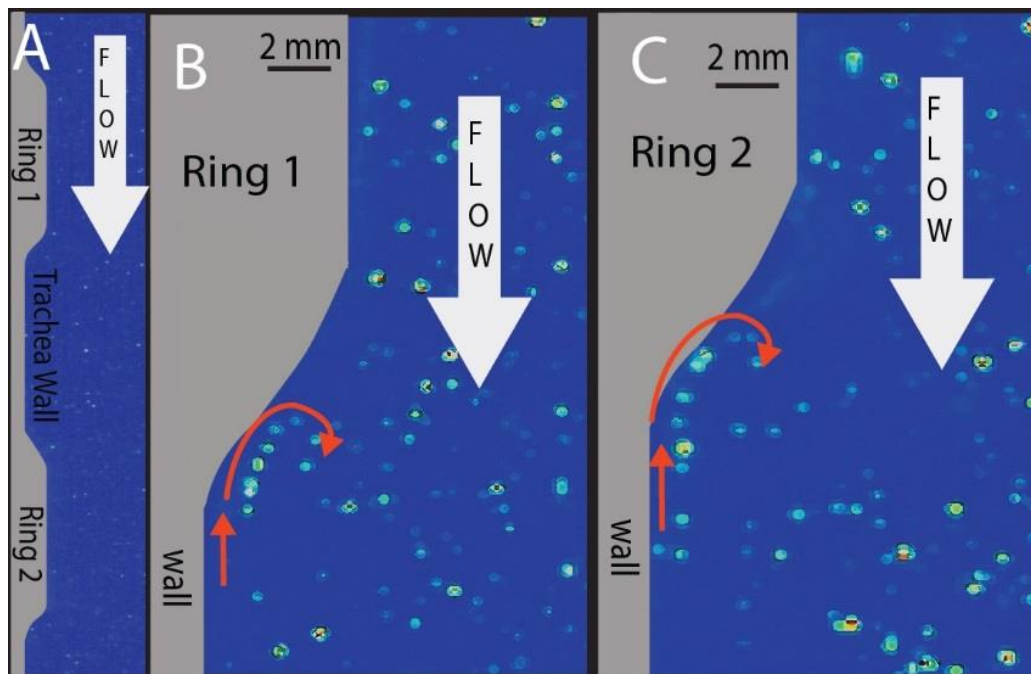
Figure 6: (A) Sample image captured for Low Resolution Data (LRD) set, with a sequence of ten superimposed images showing recirculation trajectories of particles (B&C) in the downstream side of the rings.

Thus, HRD set is analyzed with tracking of individual particles (PTV) instead of determining the velocity fields by average of windows (PIV). The velocity contour can be observed in Figure 7. Allowing a higher detail of the velocity fields and helping to understand

the physic under such phenomenon. It can be observed that the flow slows down considerably within the cavities, which is a result of the adverse pressure gradient generated by the expansion and even capture upstream velocities. A more detailed view of the cavity is shown in Figure 8, where the contour levels are limited to highlight the flow behavior near the wall. Figure 8B shows the upstream portion of the cavity with vectors, where the recirculation and displacement upstream can be observed. Figure 8C shows the downstream side of the cavity, where an acceleration of the flow can be observed due to the wall contraction.
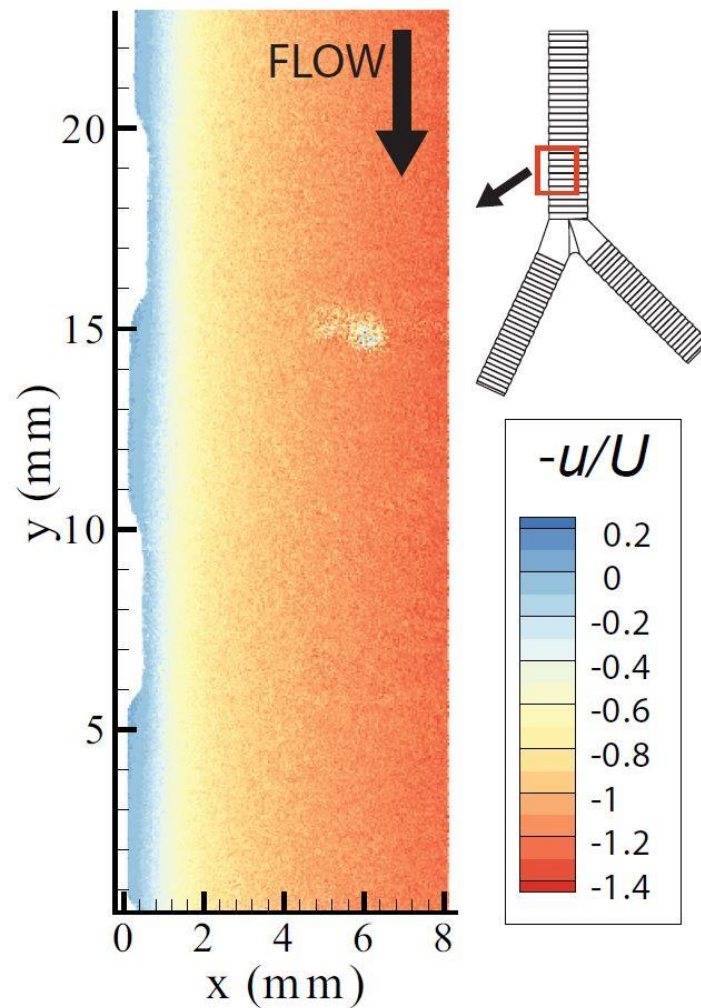
Figure 7: PTV results near the wall, at middle of the trachea model.

PTV results still does not present a clear path of recirculation because of limited resolution and particle density; however, the evidence present is enough to acknowledge the presence of these recirculation regions. Furthermore, small recirculation regions can also be

observed from studies on flow over periodic hills (Breuer, Peller, Rapp, & Manhart, 2009). Where the size of the recirculation varies from with the Reynolds number, decreasing as the Re increases. However, the recirculation reaches a minimum and increasing again, without disappearing. It is reported that the recirculation regions are related to the geometry and not much affected by the effects of the Re. Therefore, the recirculation regions in the cavities in the tracheobronchial flow is expected to be present even at higher Reynolds numbers, since our present results are at a resting breathing state conditions.
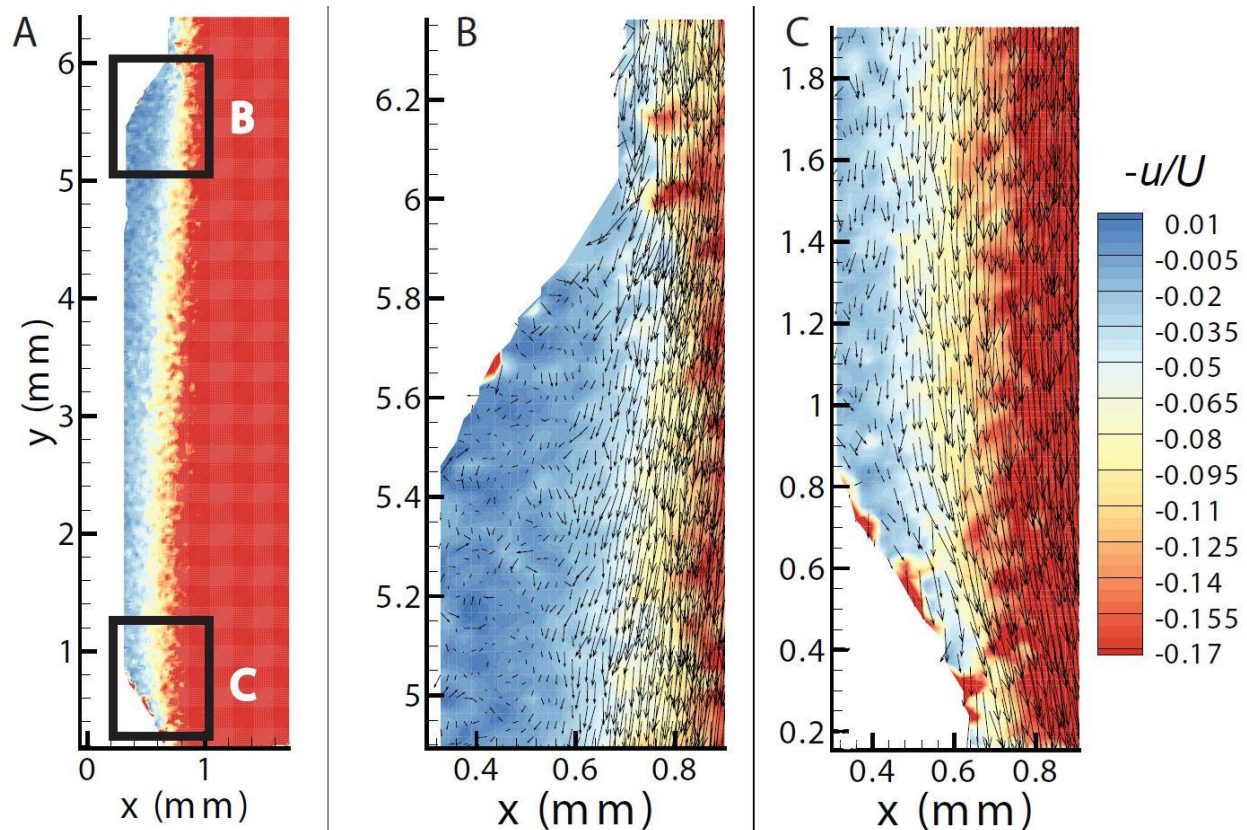
Figure 8: (A) PTV results, closer look at cavities between rings. Limited scale for detailed observation of the velocity differences at cavity. Zoomed vector field at (B) upstream side and (C) downstream side of cavity.

Both recirculation regions at the top of the cavity and acceleration at the bottom of it can affect considerably the particle deposition. In this study, the Stokes number of the tracer particles is close to cero and the densities from the fluid and the particle are practically the same. However, in aerosols for example, the density difference between the airflow and the liquid aerosol is largely different and hence, the Stokes number can have up to values ranging from 0.02 and 0.23 (Comer et al., 2001b). Because of this high difference, the denser particles cannot

follow the curved streamlines of the recirculation and are deposited. Similarly, at the acceleration in the downstream side of the cavity, the particles get deposited by inertial impaction, as also discussed by (Srivastav et al., 2013). By the results presented, we can explain the mechanisms that explain why higher particle deposition rates has been reported in previous studies (Russo et al., 2008; Y. Zhang & Finlay, 2005).

1.4. Conclusion

We presented an experimental study on a simplified tracheobronchial model to study the effect of the cartilaginous rings on the flow. In a comparison of the flow between a smooth model and a model with cartilaginous rings with high-resolution 2-dimensional data, PIV and PTV we present a phenomenon not previously known in the respiratory tract. Visual evidence present the presence of flow recirculation at the cavities between the cartilaginous rings, created by the adverse pressure gradient at the expansion of the rings to the cavities. Such phenomenon helps to explain the reason of why previous studies have found an increment on particle deposition under models that include cartilaginous rings.

The recirculation regions at the cavities creates curved streamlines, in which denser particles cannot follow and cause the particles to be deposited. Similar effect occur at the flow reattachment. At the downstream side of the rings, the flow accelerates because of the contraction of cross sectional area, and here, particles are deposited by inertial impaction. This discovery is highly valuable for drug delivery and pollutant transportation studies, since we demonstrate that the presence of the rings indeed causes a considerable difference. Hence, this study also strengthens the necessity of incorporating the cartilaginous rings in tracheobronchial models.

The models evaluated in this study are geometrically simple, to be able to isolate the effect of the presence of the rings in tracheobronchial flow. For future studies, a more complex model can be evaluated including the 3-dimensional characteristics of the flow. Along, with studies that incorporate oscillating flow (inhalation and exhalation) and to study particle deposition effect of by inertial impaction (heavier particles). This, to be able to find the optimum characteristics (particle size, shape and density) to help select an optimum delivery system for the different treatment protocols for diseases.

CHAPTER 2: TRACHEAL STENOSIS WITH CARTILAGINOUS RINGS

2.1. Introduction and literature review

Accurate knowledge of the flow characteristics in the respiratory system is vital to medical applications. For example, such as the development of treatment protocols for different diseases, in the accurate diagnosis of such and the study of particle deposition mechanics, for either pollutants or drug delivery aerosol transport. However, because of the complexity of the flow in the respiratory tract (Grgic, B., Finlay, W., Heenan, 2004; Minnich & Mathisen, 2007; Schroter & Sudlow, 1969) many studies have been developed to understand the characteristics of the flow through the years. However, because this same complexity, many of these studies have included assumptions or simplifications. Consequently, one of the most consistent simplifications in respiratory fluid dynamics research is the assumption of having smooth surface at the trachea walls (Adler & Brücker, 2007; Bauer & Brücker, 2015; Belka et al., 2014; Comer et al., 2001a, 2001b; Lizal et al., 2012; Mauder, T., Jedelsky, J. and Lizal, 2009; Ramuzat & Riethmuller, 2002; Zhao & Lieber, 1994). Where in reality the trachea are sustain by a series of cartilaginous rings, which creates depth differences in the trachea walls (Minnich & Mathisen, 2007; Russo et al., 2008).

Beside of the studies using simplified geometries for their models there has also been several studies using realistic Computed Tomography (CT) scan models (Freitas & Schröder, 2008; Grobe et al., 2007; T. Janke, Koullapis, Kassinos, & Bauer, 2019; Kim & Chung, 2009; Luo & Liu, 2008; Pedley et al., 2006). Although the CT scan captures many of the complex geometries, the limited spatial resolution neglect the smaller details. In a study made by Russo et al. (25), the researchers measured the dimensions of the rings with calipers of a whole lung specimen from a cadaver. Resulting in a ring average width of 3.21 mm, an average distance between rings of 2.98 mm and the maximum ring depth measured was 0.254 mm. The CT scan spatial resolution typically goes from 0.5 mm to 0.625 mm (E. Lin & Alessio, 2009), double the size the maximum ring depth and therefore, missing the near wall differences in height.

In order to understand how the cartilaginous rings affect the flow only few studies have been developed through comparisons of models with and without the rings (Bocanegra Evans & Castillo, 2016; Russo et al., 2008; Srivastav et al., 2013; Y. Zhang & Finlay, 2005). Russo et al.

(25) and Srivastav et al. (32) developed computational fluid dynamics (CFD) studies on the effect the rings on the flow. Russo et al. (2008) found slight differences in the flow by increasing mostly the velocity by reduction of cross sectional area; however, they do not give much detail on the fluid mechanics near the rings. Rather, in their study they focus more in the particle deposition, which found an increment of particle deposition with the rings. Srivastav et al. (2013) investigated the effect of cartilaginous rings on a tracheobronchial model based on a CT scan versus a simplified model where they found a higher shear over the cartilaginous rings. However, in this study is difficult to compare the models due to considerable geometric differences between the smooth and ringed models and the CT scan model might have also smoothed the wall, unfortunately the authors do not provide the depth of the rings to be able to compare with Russo et al.'s (2008) ring measurements. Additionally, both studies has been developed with commercial CFD-RANS (Reynolds-averaged Navier-Stokes) models, which has been reported to not be very accurate in respiratory fluid dynamics studies (Elcner, Lizal, Jedelsky, Jicha, & Chovancova, 2016; Heenan, Matida, Pollard, & Finlay, 2003; P. Koullapis et al., 2018; Mylavarapu et al., 2009; Stapleton, Guentsch, Hoskinson, & Finlay, 2000), also see Chapter 3.

Additionally, experimental studies have also been developed to understand the effect of the cartilaginous rings (Bocanegra Evans & Castillo, 2016; Montoya Segnini, Bocanegra Evans, & Castillo, 2018; Y. Zhang & Finlay, 2005). Zhang and Finlay (40) found that the presence of cartilaginous rings increase significantly the particle deposition. However, they focus only on the particle deposition and they did not measured the flow. Bocanegra Evans and Castillo (2016) showed how the rings affect the tracheobronchial flow, finding a decrease of the recirculation zones at the bifurcation of the trachea into the bronchi in the model because of the cartilaginous rings. Furthermore, in a more recent study, it was uncovered experimentally a phenomenon not previously recorded. Where is was found presence of small recirculation areas between the rings (Montoya Segnini et al., 2018). In order to comprehend better the effect of the cartilaginous rings and uncover the flow mechanics here we present a comparison of two simplified models. One model with a smooth wall and another more realistic with cartilaginous rings in a simplified pipe flow with a 70% of area contraction in the middle modelling trachea stenosis.

The obstruction in the airway ducts affects considerably the flow dynamics and the mechanics for drug delivery. Tracheal stenosis is characterized by the narrowing of the tracheal lumen, can be congenital or acquired complication of endotracheal intubation and tracheostomies

in patients (Benjamin, Pitkin, & Cohen, 1981; Spittle & McCluskey, 2000). Patients with airway narrowing usually present with different symptoms including stridor, shortness of breath, wheezing, coughing, respiratory distress or pneumonia. Often, at the point of admission to the clinic for care, the patience present loss of more than 75% of lumen has occurred (Schuurmans & Bolliger, 2004). Beside tracheal stenosis there are also other diseases that causes a contraction in the airway ducts: tracheobronchomalacia and excessive dynamic airway collapse (Benjamin et al., 1981; Murgu & Colt, 2013). This case of area contraction help us understand better the effect of the rings in the respiratory system flow.

Few numerical studies have been done in the past trying to elucidate the flow characteristics in such geometries, and none has included the cartilaginous rings. Brouns et al. (2007) showed a pressure drop in the normal breathing was only observed in cases where severe tracheal narrowing had occurred, greater than a 70% of obstruction. Hence, according to the simulations the detection of pre-critical stages of stenosis is hard to obtain by pressure differences due to only been affected at severe constriction. Similarly, Johari et al. (2012) evaluated the location of the stenosis at different locations along the trachea, determining that higher pressure and flow dynamics differences were obtain as the stenosis get closer to the bifurcation. In another numerical study, by Taherian et al. (2017), demonstrated that treatment by stent placing to treat excessive dynamic airway collapse improve the breathing condition although is not detected in a Spirometry test. Additionally, in a particle deposition study carried out a CFD simulation, experimentally validated, and showed a pressure drop and an increased particle deposition downstream of the stenosis (Taherian, Rahai, Bonifacio, Gomez, & Waddington, 2017).

Thus, in this study we analyzed with detail the effect of the cartilaginous rings near the wall and its effect on flow separation through a cross-sectional area contraction, and expansion. We compare the two models in an index-matched facility with Particle Image Velocimetry, describe in Materials and Methods. In the Results section, we present our findings and in the Discussion section, we discuss the flow dynamics over the cartilaginous rings and its effect on cases of tracheal area contraction. Finally, we share the concluding remarks in the Conclusion.

2.2. Methodology

In order to evaluate with detail the effect cartilaginous rings have on the respiratory flow we measured the flow inside two simplified trachea models with 2D particle image velocimetry (Adrian & Westerweel, 2011). Both models have a circular cross-sectional area and an axisymmetric contraction of 70% at the middle of the model. Such contraction allows to observe the effect of the rings in case airway path obstruction, e.g. tracheal stenosis, tracheomalacia and excessive dynamic airway collapse, as well, as observe the effect on flow separation, as in previous studies has demonstrated to cause differences in flow separation (Bocanegra Evans & Castillo, 2016; Montoya Segnini et al., 2018). One model has an assumed smooth wall and the other model has incorporated idealized symmetric rings, simulating the presence of cartilaginous rings, as can be observed in Figure 9. The diameter of a typical human trachea is 18 mm (Maury, 2013) and the average ring thickness, with and separation between rings are 0.254 mm, 3.21 mm and 2.98 mm respectively (Russo et al., 2008). In our models, dimension are scaled up 44% to increase the resolution of the measurements. Resulting in a diameter $D = 26.035$ mm for both models, a contraction diameter $d_c = 14.26$ mm, and for the 'ringed' model a ring thickness $t_R = 0.367$ mm, ring width $w_R = 4.64$ mm and distance between rings $w_C = 4.31$ mm.
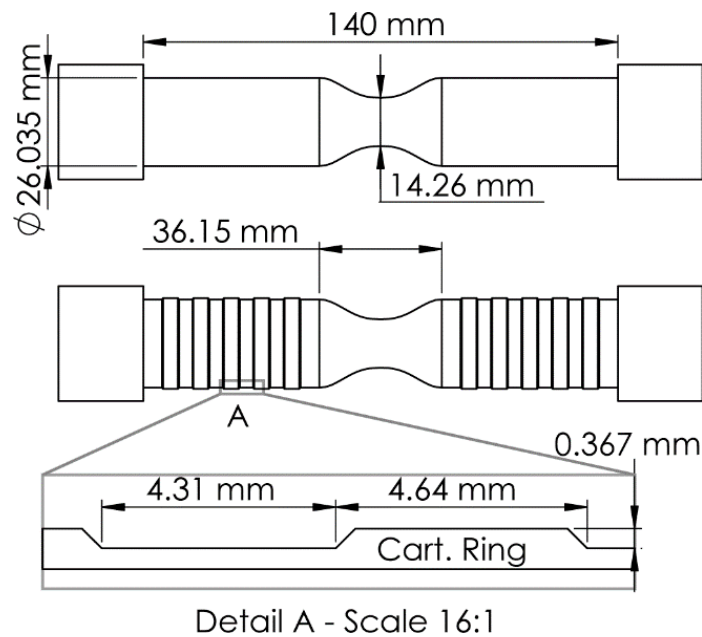

Figure 9: Trachea models dimensions for smooth (top) model and model with cartilaginous rings (bottom).

The models were created from a transparent silicone (polydimethylsiloxane or PDMS) and we used a solution of water-glycerin-salt (47.9%-37.1%-15% respectively) as working fluid. The models were submerged in a tank with the same fluid and the solution was made to match the refractive index of the PDMS ($n = 1.42$) and thus providing optical access to the flow inside the model, along with preventing user reflections when generating image closer to the wall (Shuib et al., 2010). The flow rate was based on a resting breathing state with a Reynolds number Re =3350, where the Reynolds number is a scaling non-dimensional parameter and is defined as the ratio of inertial and viscous forces (Equation (4)).

$$\text{Re} = \frac{DU}{\upsilon} \tag{4}$$

Where the kinematic viscosity of the working fluid is $\upsilon = 5.77\text{x}10^{-6}$ m^2/s, the bulk velocity is $U = 0.76$ m/s (equivalent to a flow rate $Q = 24$ mL/min) and the previous mentioned diameter $D = 26.035$ mm. The density of the solution is $\rho = 1080$ kg/m^3. Hence, since we are matching the Reynolds number the flow behavior is the same when using air. A submerged pump is used to supply a continuous inspiratory flow to the trachea model, as observed in Figure 10. The flow entering the trachea is expected to be fully developed, as a 1 meter long development region was set before the model to allow for consistency during different trials and avoid flow inconsistencies from the pump. To allow for a detailed comparison between the two models, all conditions were kept the same.
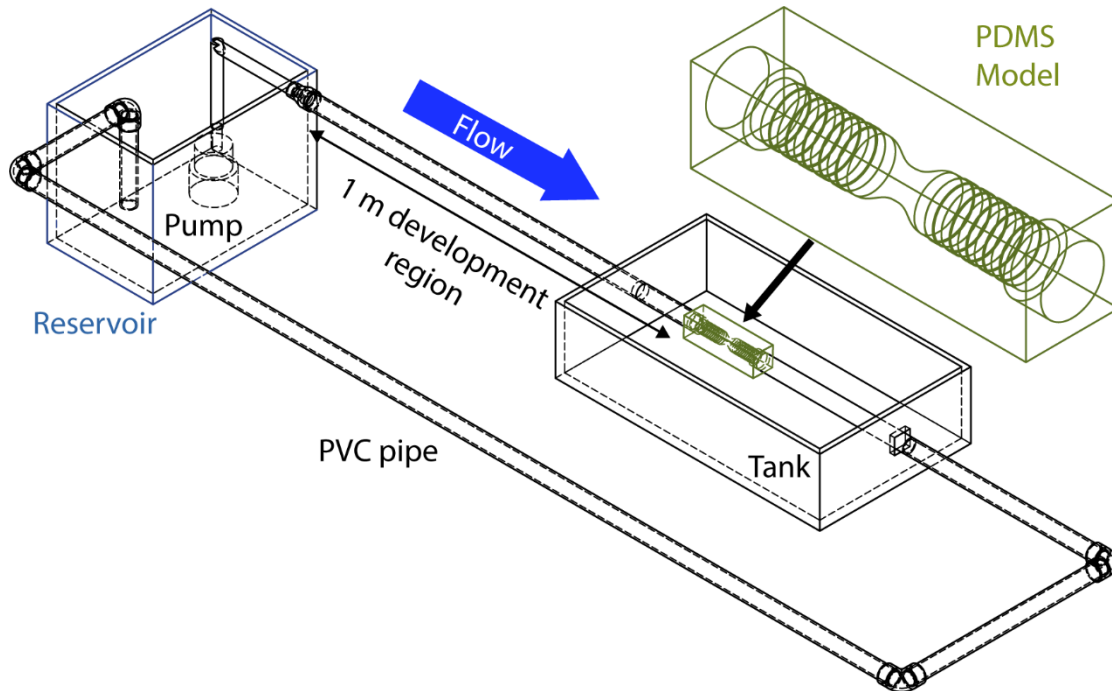
Figure 10: Experimental setup for PDMS model with Particle Image Velocimetry (PIV) evaluation.

For the fabrication of the models we designed the models in the 3D modeling software SolidWorks (SolidWorks Corporation). Afterward, we 3D printed the models in a water soluble material called PVA (polyvinyl alcohol) with an Original Prusa I3 MK2 3D printer (Prusa, Czech Republic). The 3D printed models are placed inside an acrylic container and the PDMS is poured in the container with the PVA part. Once the PDMS is cured, the model taken out of the acrylic container and is submerged in water for the 3D printed core to be dissolved.

We used a 2D planar PIV system to analyze the flow. The PIV system consist of an 8-bit CCD camera with resolution of 4008×2672 pixel^2 and a Nd:YAG 532 nm laser used to illuminate the tracing particles. The particles used are made of a polyamide fluorescent with a diameter of 15 μm and density of $\rho = 1100$ kg/m^3 (Kanomax, New York). As explained in a previous study, the particles can be considered tracers that accurately follow the flow (Montoya Segnini et al., 2018). We used lenses to create a thin sheet layer of 1 mm to illuminate the particles, the thin sheet is located at the center of the model along the streamwise direction. We captured a window before and after the contraction (including the contraction in both cases) with a resolution of 59.7 pixels/mm. For each window we collected 1500 image pairs with time difference between frames of 210 μs. Every pair is processed with a multi-pass PIV algorithm

(LaVision). We used an initial interrogation window of 96×96 pixel^2 and a final pass with 48×48 pixel^2 with a 50% of overlap.

2.3. Results and Discussion

Velocity contours were obtained from the 2D-PIV experiments for both the smooth model and the 'ringed' model, see Figure 11. Velocity is normalized by the maximum velocity in each model. Since the model is symmetric, same behavior is expected in all directions. For both models, an acceleration of the flow is noted at the contraction, as expected from the decrease of cross-sectional area, and at the expansion flow separations occurs, as was also reported to occur by Brouns et al. (2007). The separation observed is produced by the adverse pressure that occurs at the expansion of the cross-sectional area. Similar velocity is observed before the contraction and a similar acceleration occurs at the contraction, however the most notable difference between cases is found on the separation after the contraction. The smooth model has a bigger and stronger flow separation than the model with rings. As can be observed in Figure 11, the smooth separation region is darker than the 'ringed' one.
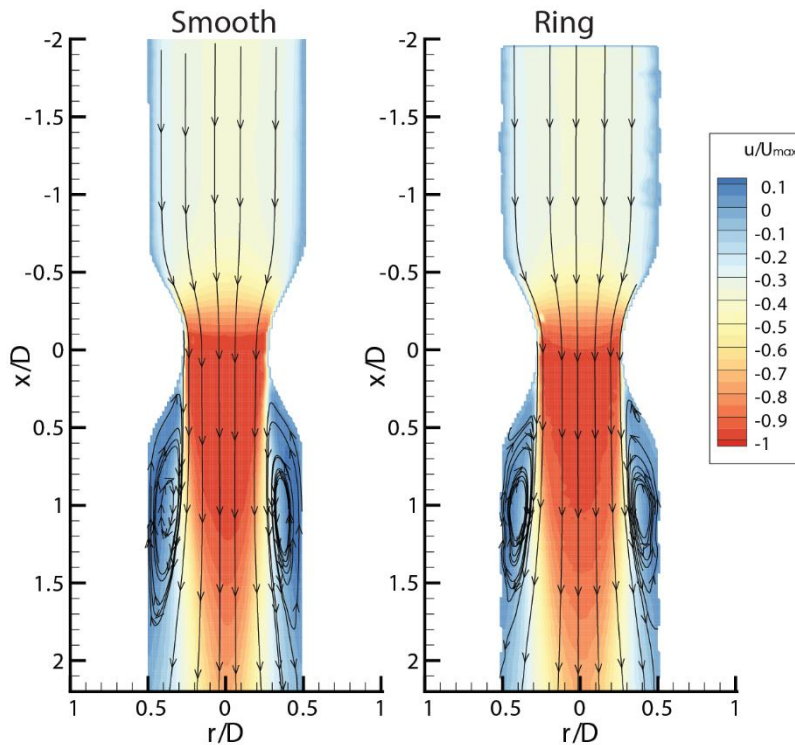
Figure 11: Particle Image Velocimetry (PIV) results: Velocity contours for Smooth model and model with Cartilaginous Rings.

The smooth model has a recirculation length of 43.74 mm and the ringed model a recirculation length of 39.05 mm, reducing the length by 10%. To understand better the effect of the cartilaginous rings we analyze the velocity profiles of both cases (Figure 12Figure 11: Particle Image Velocimetry (PIV) results: Velocity contours for Smooth model and model with Cartilaginous Rings). The velocity profiles are extracted at five different locations. From the upstream side of the contraction we have an inlet position at two diameter (-2D) before the middle of the contraction and another at -0.75D. In the downstream side of the contraction, at 0.5D, 1D and 2D to study the differences of the flow separation. From both profiles before the contraction, we can observe that the flow is practically the same for both cases, which mean that the inlet flow for both cases is the same and that the rings do not cause significant differences on the velocity profile. Nevertheless, the flow after the contraction is different between cases.

As noted from the velocity contours in Figure 11, the separation region is stronger for the smooth case. In the model with cartilaginous rings the flow separation is delayed and it can be noticed a smaller separation bubble at 0.5D and at 1D. At 0.5D, the separation bubble of the model with rings is 3% smaller than the smooth model, which means the separation is occurring before on the smooth model. After the contraction, at 1D the separation continues to be smaller for the 'ringed' model. Along with the differences in size, the intensity of the recirculation is also distinct. The effect of the rings reduces 38% the maximum upstream velocity at the separation region. Similar results of recirculation reduction have also been reported in the separation region at the bifurcation from the trachea to the bronchi (Bocanegra Evans & Castillo, 2016; Montoya Segnini et al., 2018).
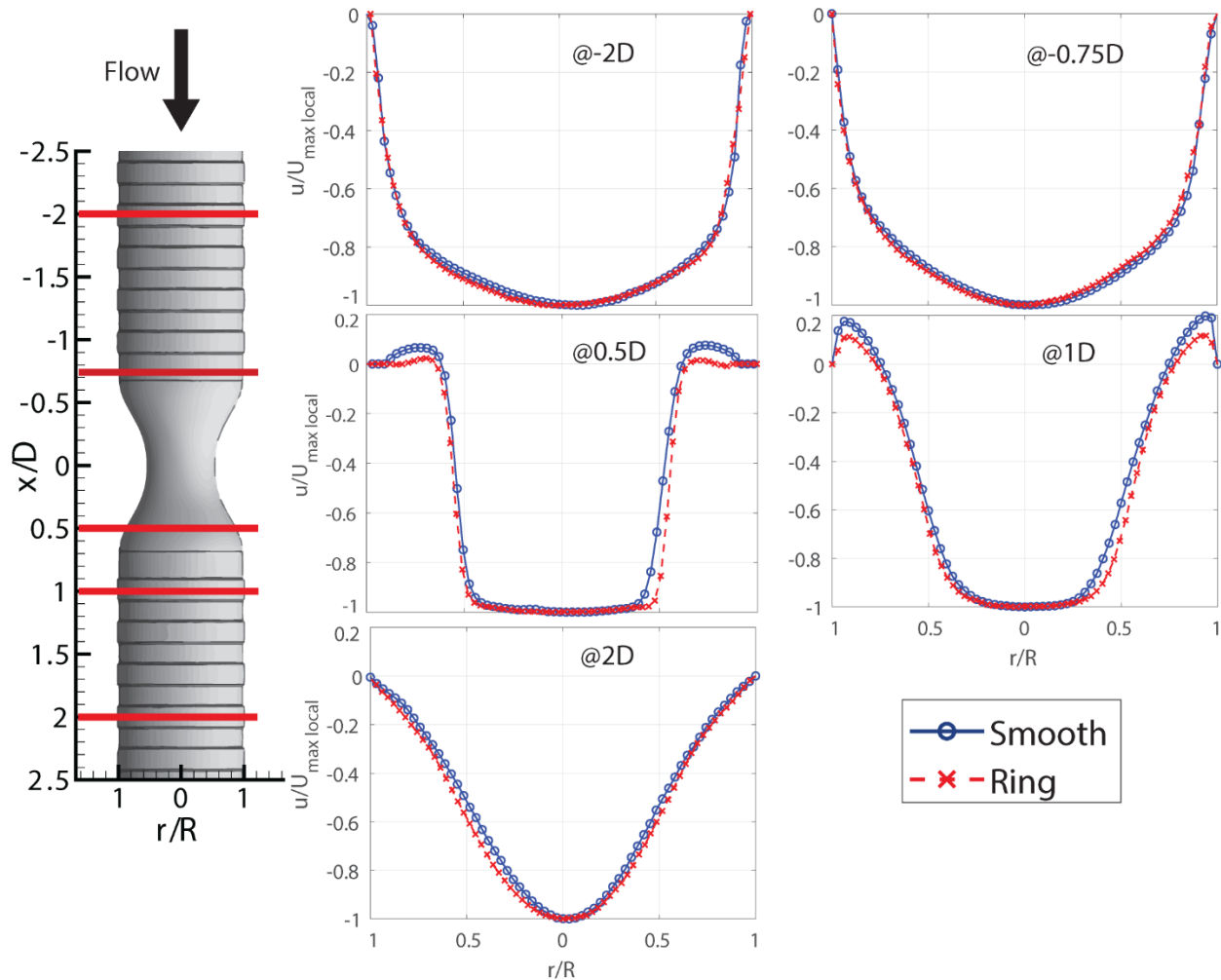
Figure 12: Velocity profiles from PIV results (velocity is normalized by maximum local streamwise velocity).

In order to understand the phenomena producing this differences in the flow separation between models we observe with more detail the upstream side of the contraction. Although the velocity profiles between models are practically the same (Figure 12), the separation regions are very distinct. Hence, we observe at the velocity fluctuations occurring near the walls of the models. Because of a small bubble reflection we are not allowed to obtain an accurate value of fluctuations at the top of the model. However, we obtain the values of fluctuations at 1.5 diameters (-1.5D) before the contraction and at -0.75D, see Figure 13. We evaluate the streamwise Reynolds stresses (u'^2/U^2_{max}) and the Reynolds Shear stresses (uv/U^2_{max}), both normalized by the maximum local velocity.

The production term (P), described in Equation (5), of Turbulent Kinetic Energy (TKE) is defined by the fluctuations from the streamwise flow (u'), the wall normal flow (v') and the rate of length from the wall ($\partial U/\partial y$).

$$P = u'v'\frac{\partial U}{\partial y} \tag{5}$$

In this study, we compared the normalized streamwise flow (u') and the wall normal flow (v') between cases, which is proportional to the production term.
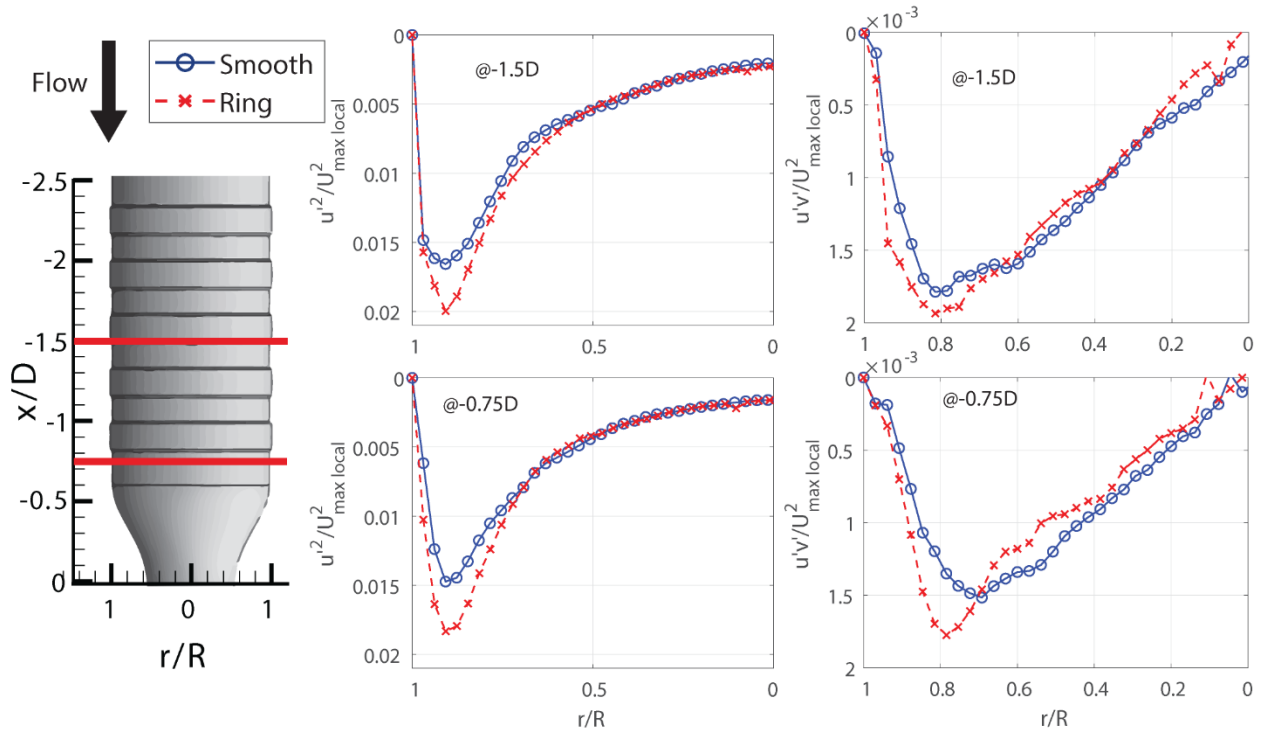
Figure 13: Streamwise Reynolds stresses and the Reynolds shear stresses upstream of the contraction (normalized by the maximum local velocity).

As observed in Figure 13, both the streamwise Reynolds stresses and the Reynolds shear stresses differences between models increase as the flow goes downstream. At -1.5D, the streamwise Reynolds stresses is increased by 20% because of the rings, which occurs after going over three rings. Closer to the contraction at -0.75D the difference is increased to 24%. Likewise, the Reynolds shear stresses increased by 8% at -1.5D and 17% at -0.75D. These differences are due to the increase turbulence production occurring at the rings, the smooth model fluctuations stay constant along the model, contrary to the 'ringed' model, in which the turbulence increases.

This occur because the rings are generating perturbations to the flow, as was also reported in the tracheobronchial flow study (Bocanegra Evans & Castillo, 2016). Such perturbations caused by the cartilaginous rings transition the boundary layer to turbulent and enhances the near-wall momentum, resulting in less separation than a more laminar flow (Choi, Jeon, & Kim, 2008). As the cartilaginous rings reduce the separation, it also reduce the fluctuations and turbulence downstream of the contraction. As observed in Figure 14, the turbulent kinetic energy is reduced in the case of the 'ringed' model. With a larger separation bubble the shear layer increases in size generating higher fluctuations.
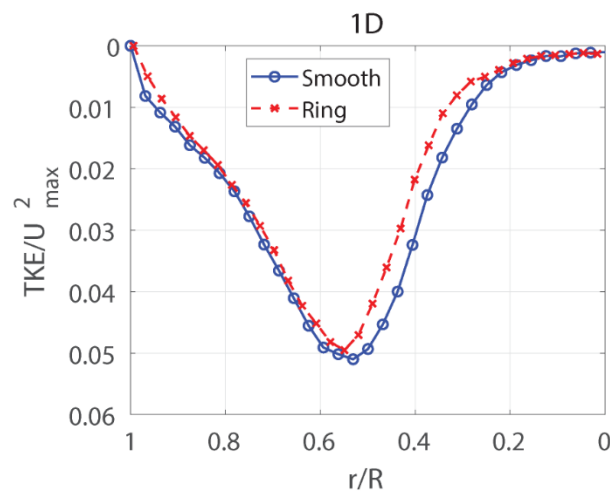
Figure 14: Turbulent Kinetic Energy (TKE) at one diameter (1D) after the contraction (normalized by the maximum velocity at the contraction).

In previous studies, it has been demonstrated that cartilaginous rings reduce the separation at the bifurcation (Bocanegra Evans & Castillo, 2016; Montoya Segnini et al., 2018). Where it was speculated that the rings are inducing disturbances in the flow. Equally, in this study we detect a decrease of the flow separation. However, here we present evidence of the cartilaginous rings disturbing the flow and creating fluctuations and turbulence to the flow. As the flow goes along the model with rings the fluctuations increase and eventually reducing the separation in the flow. Similarly, in previous studies it causes consequences downstream of the separation. Because the separation is reduced, the separation region is smaller and the shear layer is reduced. By reducing the shear layer, the mixing of the flow is also reduced and the flow is less turbulent downstream.

In an analysis of pipe flow over periodic surface roughness it was determined that the presence of such leads to a periodic fluctuation on the flow (Song, Yang, Xin, & Lu, 2018). Leading to pressure drop across the pipe. Similarly, in our model we observe an increase of fluctuations. Although we did not performed pressure measurements, we can expect a similar behavior in an increase in pressure drop along the trachea. However, the length of the trachea is small and would not have a considerable effect. Nevertheless, the fluctuations generated by the rings are strong enough to cause a considerable difference on the separation. Leading to possible higher effects on the consequent branching generations in the respiratory tract.

Previously it was recorded the presence of recirculation regions after the rings (Montoya Segnini et al., 2018). Such phenomenon increases the particle deposition by the particles not been able to follow the curved streamlines and to be deposited by inertial impaction. Similarly, for the acceleration occurring before the rings because of the cross-sectional area reduction. Additionally, as the flow near the wall becomes more turbulent it promotes the particle deposition locally as the flow fluctuation will increase the particle deposition (P. G. Koullapis, Kassinos, Bivolarova, & Melikov, 2016). Regarding the separation reduction on particle deposition, Zhang and Finlay (2005) reported an increase in particle deposition along the trachea but not does not affect the bronchi. Similarly, Russo el al. (2008) found particle deposition increase along the trachea but not considerable differences at the bifurcations. This, because by reducing the separation region the particles will be less prone to get deposited at the separation regions, though, the higher turbulence downstream it will consequently increase the particle deposition.

As previously mentioned, Brouns et al. (2007) found that pressure drop was only found under sever constriction, which difficult the diagnosis of disease from before getting constriction over 70%. The delayed separation occurred by the rings reduce even more the pressure reduction and hence, the diagnosis of the disease. In addition, the particle deposition in trachea stenosis cases can be affected by the decrease of flow separation, since is going to have less separation area and less mixing downstream. Such effect can also be related to the findings of Bocanegra and Castillo (2016), where less vorticity was found for the rings due to the reduction in flow separation at the bifurcation.

2.4. Conclusion

We analyzed the effect of the cartilaginous rings in the respiratory system with a stenotic case of a 70% area contraction. The comparison was developed between two models, one with a smooth wall surface and other with modelled cartilaginous rings. We observed similar flow field before the contraction but the main velocities differences were found downstream of the contraction. Where, separation region was reduces considerably by the 'ringed' model. The cartilaginous rings perturb the flow near the wall by increasing the fluctuations and hence, delaying the separation at the expansion.

The most important message from these results is that even though not notable differences are observed in the velocity fields of the flow, is that the rings give small fluctuating differences causing a considerable difference on the flow separation. Thus, its importance to include the cartilaginous rings in respiratory system fluid dynamics studies, including mostly particle deposition research. While our model is a very simplified shape, comparing to actual human respiratory system complex geometry, our results allow us to isolate the effect the cartilaginous rings have on the flow. Future studies should be made to study the effect of the delayed separation in consequent generations to be able to observe how much it differs from the smooth models previously studied.

CHAPTER 3: EVALUATION OF RANS CFD IN RESPIRATORY FLOW

3.1. Introduction and literature review

As observed through the studies discussed in both Chapter 1 and Chapter 2, many of them have been done by numerical simulation. Given the complexity of the flow, difficulties to measure and capture all characteristics, and the computational capacity increase, numerical simulation has been an important tool to understand the flow mechanics and particle deposition in the respiratory system flow. One of the ultimate goals of respiratory fluid dynamics research is to be able to develop patient-specific treatment for their distinct needs (Kleinstreuer & Zhang, 2010), as geometrical conditions and strengths can vary considerably from patient to patient. This can be achieved by developing personalized models obtained from non-intrusive imaging methods like Computer Tomography Scan (CT scan) or Magnetic Resonance Imaging (MRI) to obtain all the anatomical characteristics of a patient's respiratory tract. Later, use the model developed and use numerical simulation to capture the flow characteristics through Computational Fluid Dynamics (CFD).

To be able to achieve the goal of personalized treatment through CFD, computer simulations has to be accurate enough to capture all flow characteristics for the given patients, it has accessible to caregivers (avoiding the necessity of supercomputing) and to be able to run relatively fast. These needs have led researchers to develop simplified mathematical models to simulate the flow for different applications, among them the flow inside the respiratory system. Although CFD has become a groundbreaking tool in fluid dynamics studies is has its own limitations, hence, in this chapter we discuss the importance of validation of computer simulations of the flow dynamics in the respiratory system. It is important to understand such limitations in order to improve models toward a personalized medicine. In CFD, there are three main approaches for simulating turbulent flows: Direct Numerical Simulations (DNS), Large Eddy Simulations (LES) and Reynolds-Averaged Navier-Stokes (RANS) models.

DNS solve the full Navier-Stokes (NS) equations, resolving all scales of fluid motion. DNS is the most accurate technique, and has been used to study the respiratory flow, being able to find good agreement with experimental validation (Ball, Uddin, & Pollard, 2008; C. L. Lin et al., 2007; Raiesi, Piomelli, & Pollard, 2011). However, DNS is computationally expensive

(requiring the use of super-computing) and time consuming. Similarly, LES solve the NS equations by direct computation but only the large scales of motion, the small scales are modeled. LES has also been used extensively in the respiratory flow (Bernate, Geisler, Padhy, Shaqfeh, & Iaccarino, 2017; Chen & Gutmark, 2014; Gutmark, 2015; T. Janke et al., 2019; Raiesi et al., 2011). Even though is less costly than DNS it is still considered relatively computationally expensive (Bailly & Comte-Bellot, 2015). Both techniques, DNS and LES, have demonstrated to be accurate, yet computationally expensive to consider patient specific evaluation.

In contrast to DNS and LES, RANS models solve time-averaged NS equations, which reduces considerably the computational cost (Pope, 2001). Making possible to run the simulations in workstations and even in some modern laptops. RANS models are widely used due to its low computational cost, including in respiratory fluid dynamics research. Where the most used variations are the two-equation models k-ε (which solves the Reynold stresses and the dissipation) and k-ω (Reynold stresses and turbulent length scale) and their extensions (to be discussed in the methodology). In this chapter, it is evaluated the accuracy of RANS models simulations in the respiratory flow through a comparison of high-fidelity experimental data and several RANS models to demonstrate and understand the limitations of such.

Currently, RANS simulations are extensively used on the investigation of respiratory flow. Such models are used to comprehend the flow through complex geometries such as the extra-thoracic airway, for example to model the wall shear stress (Green, 2004). Additionally, identifying the flow differences with and without small geometrical perturbations, like on the presence of cartilaginous rings (Russo et al., 2008; Srivastav et al., 2013). On the evaluation of the flow with respiratory diseases that give path obstruction of the flow, like tracheal stenosis (Brouns et al., 2007; Taherian, Rahai, Gomez, et al., 2017). In addition, in particle deposition investigations as well (Li, Kleinstreuer, & Zhang, 2007).

Although, RANS models are convenient to use due to its economical computational value is already known to have some limitations (Brooke, Hanratty, & McLaughlin, 1994; Coleman, Rumsey, & Spalart, 2018; Raiesi et al., 2011). Moreover, this has been the case for most of RANS studies that have compared their numerical results with experimental data in respiratory flow dynamics. Beginning with a previous study by Heenan, Matida, Pollard, and Finlay (2003), where in a comparison between their experimental measurements with RANS simulations of an

idealized human oropharynx were able to find discrepancies. Even though the simulations were able to capture the basic features of the flow, the simulations were not able to capture accurately the fluid motion near the wall at low Reynolds numbers. Similarly, Mylavarapu et al. (2009) compared different RANS models (k-ε, k-ω and k-ω SST (Shear Stress Transport)) to experimental measurements. Comparing pressure measurements, the best agreement reported was in case of the standard k-ω model, with 20% of average error, which means the other models had even higher error.

In a more recent study by Elcner et al. (2016), good agreement was found in the velocity profiles in several cross sections between experimental and simulated results. However, the RANS simulations struggle to predict the separation regions in the locations with large curvature. Similarly, in studies of particle deposition comparison of flow simulation and experiments a great difference has been found. In a numerical study by Stapleton et al. (2000), although they found good agreement in particle deposition for laminar flows, for turbulent flows the particle deposition rate was up to three times higher than experimentally measured values. Likewise, Koullapis et al. (2018) found in their comparison that RANS simulations overpredicted deposition of small and intermediate particle sizes and underpredicted that of large particle sizes. Hence, in this chapter we evaluate the limitations of commercial simulation algorithms by testing a simple trachea model experimentally versus numerical simulations using various RANS models.

3.2. Methodology

In order to evaluate the accuracy of several RANS models we compared the experimental results from the PIV measurements, described in Chapter 2, and compared them to our numerical simulations. As previously described, the model is tested under well-controlled laboratory conditions. The model compared in this evaluation is the model with cartilaginous rings, which we have argued in Chapter 1 and 2 the importance to include them in respiratory flow studies. This due to the effect to the flow near the wall and the size of flow recirculation zones downstream (Bocanegra Evans & Castillo, 2016; Montoya Segnini et al., 2018; Russo et al., 2008; Srivastav et al., 2013). Details of the experimental setup are described in Chapter 2 and dimensions of the model can be observed in the schematic in Figure 15.
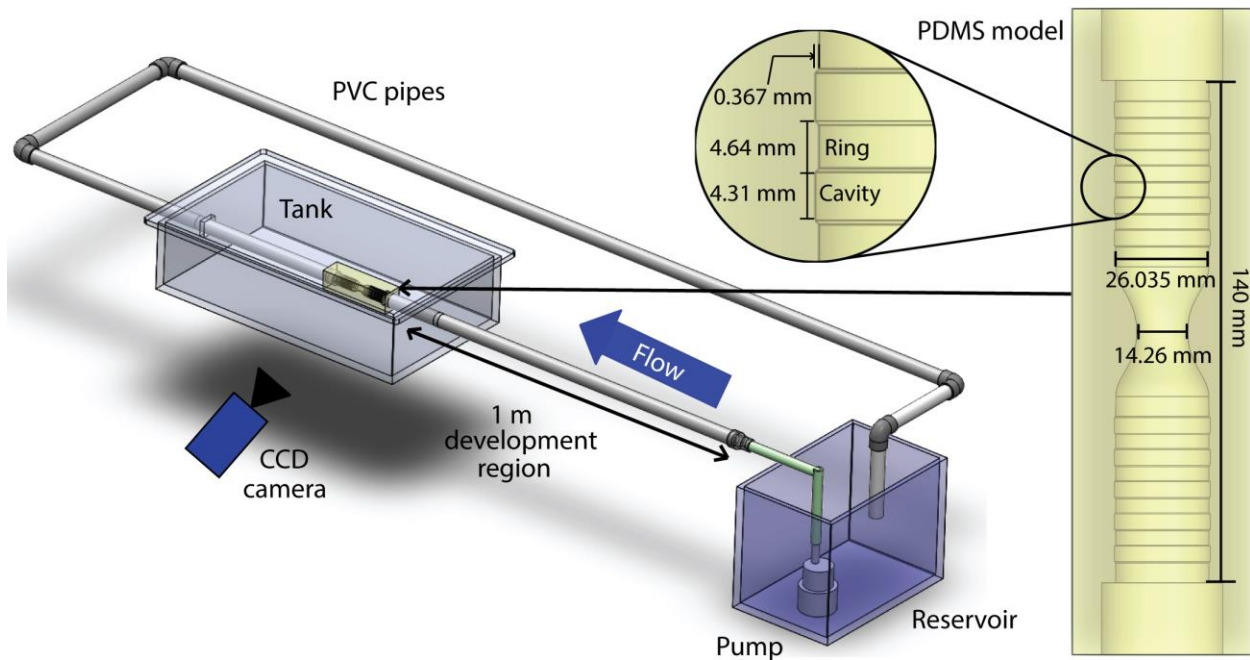
Figure 15: Dimensions of cartilaginous ring model and schematic diagram of the experimental setup.

We carried numerical simulations in an identical trachea model where we used several RANS models. We evaluate the two–equation model $k - \varepsilon$ and its extension the $k - \varepsilon$ RNG (renormalization group), used in several respiratory studies (Brouns et al., 2007; Green, 2004; Srivastav et al., 2013; Stapleton et al., 2000). Along with the two–equation model $k - \omega$ in standard, SST (Shear Stress Transport) and SST LRN (Low–Reynolds number) variations (Heenan et al., 2003; Li et al., 2007; Mylavarapu et al., 2009; Russo et al., 2008; Taherian, Rahai, Gomez, et al., 2017). In addition, an evaluation with 4-equation Transition SST. All used models are from ANSYS FLUENT commercial software, with a second-order discretization scheme. The structured grid of the 3-D domain contained 315,000 cells, with grid independence test performed. The inlet velocity profile was imported from experimental results with measured turbulence intensity $T_{u\%} = 6\%$ and with a pressure outlet boundary condition.

3.3. Results and Discussion

As observed from the results in Chapter 2 and in Figure 16, the flow accelerates as it gets closer to the contraction and at the expansion, separation of the flow occurs which are the negative velocity near the wall caused by the adverse pressure gradient. Similar results are

observed from the numerical simulations at all models tested with clear separation regions at the expansion. In Figure 17, the velocity field contours can be appreciated for the PIV results and the numerical simulations for k-ε, k-ω, k-ω sst and the 4 equation transition model. Although similar inlet conditions are present and separation is present in all models, clear differences are observed between all the contours, as observed in the lower velocity field contours in Figure 17. To have a better understanding of the differences the velocity profiles are shown at four different locations within the model in Figure 18: inlet profile (*x/D* = -2), at and after the expansion (*x/D* = 0.5 and 1), and downstream (*x/D* = 2).
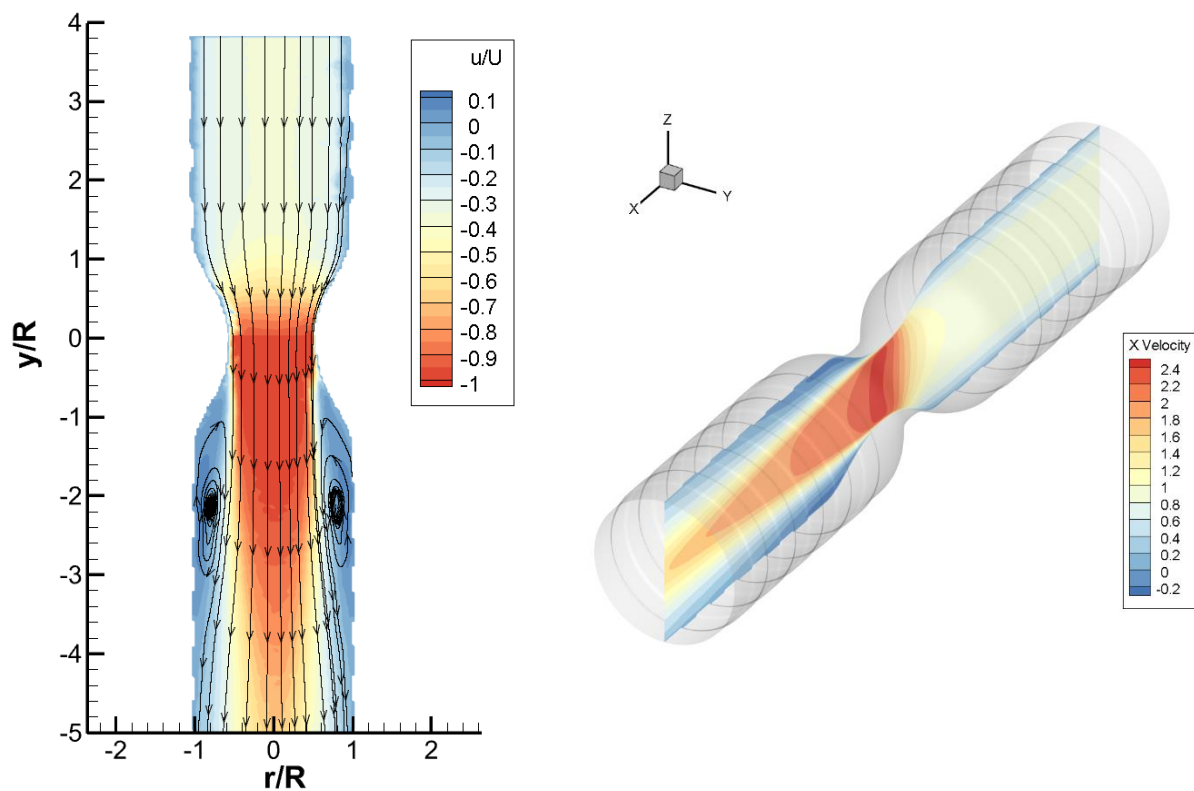

Figure 16: (Left) PIV results and (right) CFD results..

PIV   k − ε   k − ω   k − ω sst   k − ω sst tran 4eq
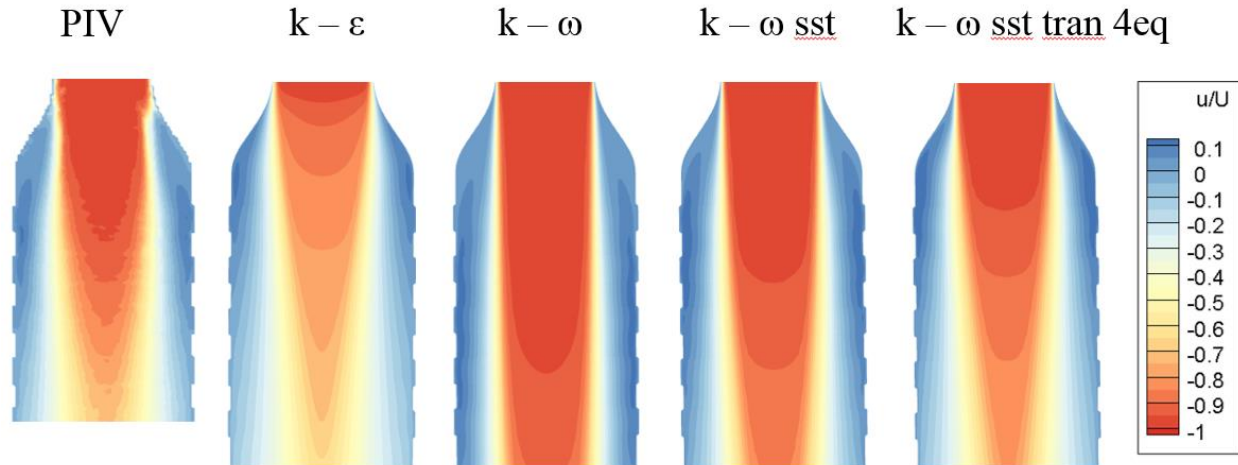
Figure 17: Velocity field contours for experimental PIV results and computer simulations k-ε, k-ω, k-ω sst and the 4 equation transition model.

As observed in all the inlet velocity profiles (x/D = -2) before the contraction, the flow is almost identical for all cases, meaning we have similar entrance conditions for experiments and simulations, where turbulence intensity is also matched. While all cases show clear recirculation areas, their size, shape and strength differ significantly from each other. Velocities, in Figure 18, are normalized by the maximum experimental streamwise velocity ($u/U_{max, exp}$) and the profiles at subsequent locations are shifted by one unit. Along with the velocity profiles, the recirculation sizes of the different models are presented in Figure 19 and Figure 20, where the velocities moving upstream are denoted by the amount of area marked.

Although inlet velocity profiles are identical, differences can be noted immediately after the contraction (x/D = 0.5) for the k − ε and k − ε RNG models, where separation clearly develops earlier for the simulations. The k − ε model is known to have poor prediction of flow separation (Raiesi et al., 2011). At x/D = 1, the k − ε model already presents disparity with the experimental measurements. Even though the separation region has a similar width as the experiments, the magnitude of the flow velocity moving upstream is 35% lower than the experimental data. To maintain the overall flow rate, the flow moving in the middle is 10% slower than in the experiments. At 2D the differences remain present, while the RNG model presents a better agreement. Such differences would affect the particle deposition greatly.
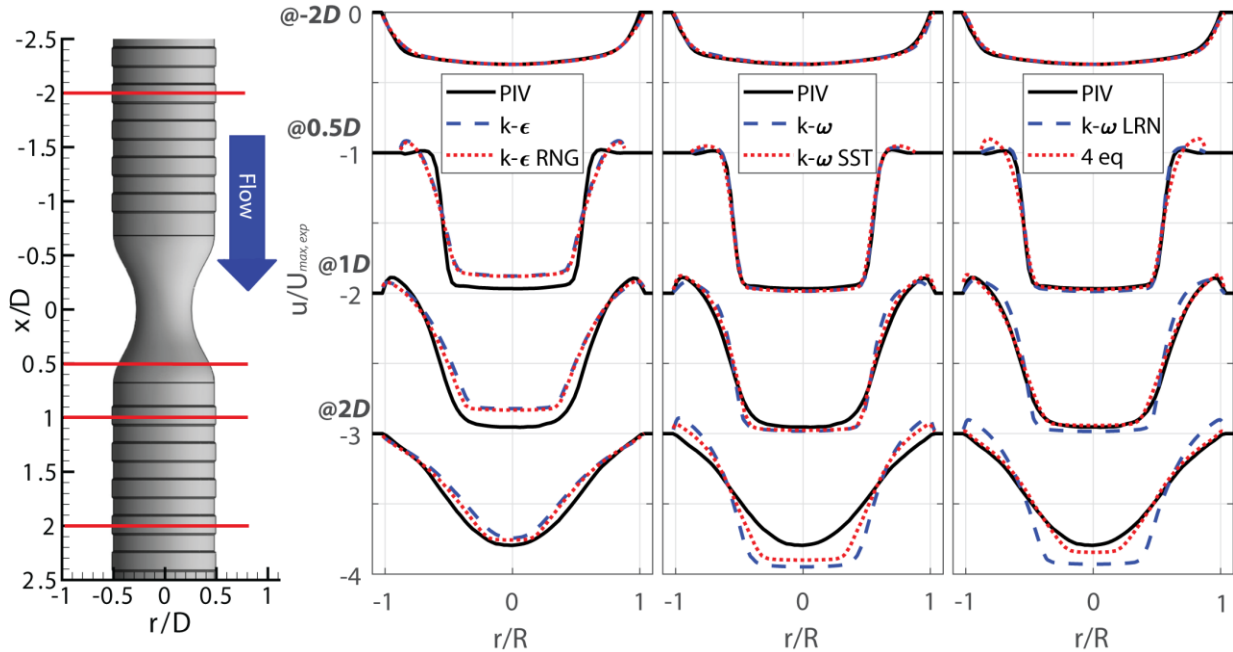
Figure 18: Experimental (PIV) measurements vs. simulation (CFD-RANS models) comparison: $k-\varepsilon$, $k-\varepsilon$ RNG, $k-\omega$, $k-\omega$ SST, $k-\omega$ SST LRN and 4-equation Transition SST, from left to right.

The $k-\omega$, $k-\omega$ SST and $k-\omega$ SST LRN results are similar to the experimental measurements at $x/D = 0.5D$ and $1D$, and differences between these models are small. However, at $2D$ the separation remains present for the simulation but has reattached in the experiments. It is particularly worrisome that the differences increase as the flow moves downstream, since such large error could propagate into the ensuing generations. Results are consistent with the study made by Coleman et al. (2018) for RANS models, where it is shown that the $k-\omega$ SST model, along with most other RANS models, predict the separation point accurately but there is significant error in the reattachment point. Also observed in Figure 17, where reattachment is not even visible in the model length. These models are shown to overpredict the length of the separation bubble, as we see in our case (shown in Figure 18 at $x/D = 2D$), but the underlying cause remains unclear (Coleman et al., 2018).

The best agreement is found for the 4-equation transition SST model, where although the separation occurs earlier at the expansion ($x/D = 0.5D$), the reattachment of the flow is close to the experimental observation. The velocity agreement at $x/D = 1D$ and $2D$ is good, with a 2.77% and 4% of error respectively. Resulting in a better agreement for the flow downstream than the other models. The 4-equation transition mode is based the $k-\omega$ SST transport equations coupled

with two other transport equations, intermittency and a transition momentum thickness Reynolds number (Langtry & Menter, 2009), presenting excellent results in flow separation in previous benchmark studies (Menter, Langtry, Völker, & Huang, 2005).
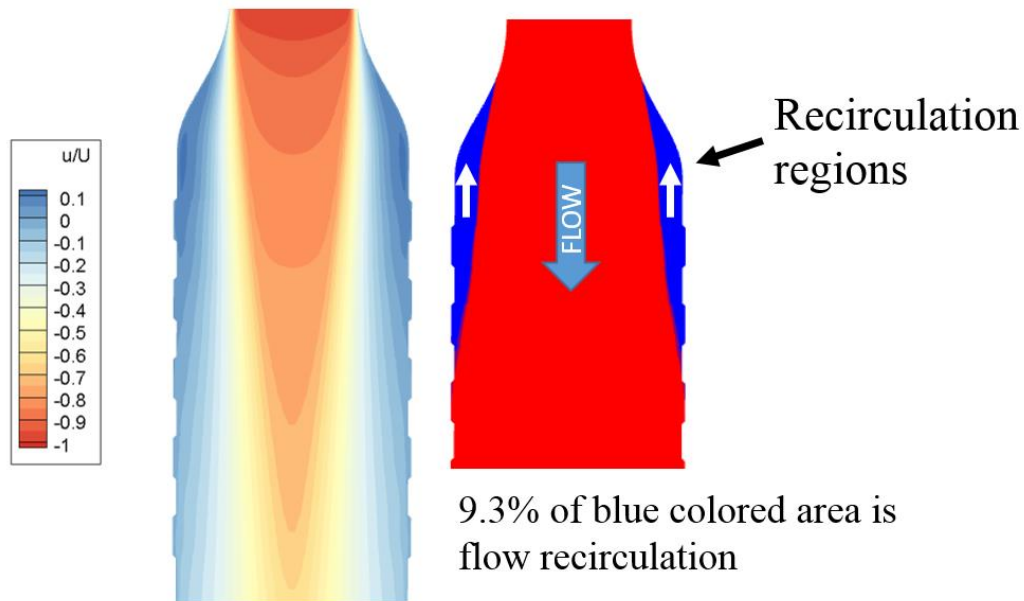
Figure 19: Area percentage determination downstream of contraction.
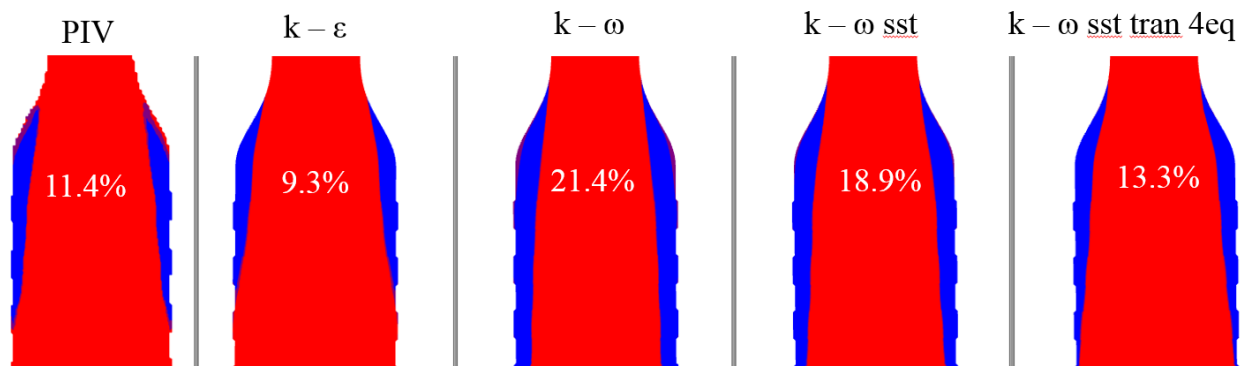

Figure 20: Recirculation area percentage for experimental PIV results and simulated k-ε, k-ω, k-ω sst and the 4 equation transition model.

Percentage of recirculation area is observed in Figure 20. Although the $k - \omega$ models did not even shown the reattachment point for the given length, we still compared the size difference of the area of the regions.

Our trachea model is significantly simpler than actual human tracheae, leading to the conclusion that RANS is not a reliable tool in respiratory fluid dynamics (with relative exception of the 4-equation transition model), particularly in areas with complex geometrical features. Considering the overall geometry of the respiratory tract (repeated bifurcations without fully developed flow), inaccuracies in the upper generations will continue to propagate and increase the error in the subsequent generations. Furthermore, our data, and other data available in literature, exhibit larger discrepancies near the walls, making RANS an unreliable tool for particle dispersion and deposition studies, given this phenomenon is largely influenced by the flow conditions near the boundaries (Brooke et al., 1994).

3.4. Conclusion

Even though some studies validate the simulation results with experiments, the RANS simulations can change behavior considerably at different Reynolds numbers and geometric modifications, resulting in miscalculation from the simulations with different parameters. On the contrary, DNS and LES simulations were found to be more accurate in respiratory fluid dynamics studies (Bernate et al., 2017; Chen & Gutmark, 2014; T. Janke et al., 2019; C. L. Lin et al., 2007), but at significantly higher computational cost.

Given the geometric and flow characteristics of the respiratory system, it appears that the traditional RANS algorithms, as they currently stand, are not reliable for research in respiratory fluid dynamics. It is therefore necessary to develop mathematical models that more accurately represent the flow within the airway. To develop these models, however, we need a better understanding of the flow physics, which requires high fidelity data from experiments or direct numerical simulations.

CONCLUSION

In order to understand the effect of the cartilaginous rings in the tracheobronchial flow it was developed two two experiments on trachea models. Both experiments, developed in a refractive-index matched setup to have complete optical access of the model, even very close to the walls, and analyzed with Particle Image Velocimetry (PIV). Furthermore, both experiments had one model with smooth walls and other with the presence of cartilaginous rings. The first experiment was on a simplified tracheobronchial model, with the trachea and main bronchi. We captured high-resolution 2-dimensional data and used both PIV and PTV to analyze it.

In this experiment, we present a phenomenon not previously known in the respiratory tract. Visual evidence present the presence of flow recirculation at the cavities between the cartilaginous rings, created by the adverse pressure gradient at the expansion of the rings to the cavities. Such phenomenon helps to explain the reason of why previous studies have found an increment on particle deposition under models that include cartilaginous rings. The recirculation regions at the cavities creates curved streamlines, in which denser particles cannot follow and cause the particles to be deposited. Similar effect occur at the flow reattachment. At the downstream side of the rings, the flow accelerates because of the contraction of cross sectional area, and here, particles get deposited by inertial impaction.

In the second experiment, we analyzed the effect of the cartilaginous rings in the respiratory system with a stenotic case of a 70% area contraction. We observed similar flow field before the contraction. However, the 'ringed' model reduced the separation region considerably after the contraction. We observed that the cartilaginous rings perturb the flow near the wall by increasing the fluctuations and hence, delaying the separation at the expansion. Having the presence of the rings a considerable difference in separation is important to consider then doing studies that include a contraction, since this is where higher differences are present.

The models evaluated in this study are geometrically simple, to be able to isolate the effect of the presence of the rings in tracheobronchial flow. Both experiments presented are highly valuable for drug delivery and pollutant transportation studies, since we demonstrate that the presence of the rings indeed causes a considerable difference. Hence, this study also strengthens the necessity of incorporating the cartilaginous rings in tracheobronchial models.

For future studies, a more complex model can be evaluated including the 3-dimensional characteristics of the flow. Along, with studies that incorporate oscillating flow (inhalation and exhalation) and to study particle deposition effect of by inertial impaction (heavier particles). This, to be able to find the optimum characteristics (particle size, shape and density) to help select an optimum delivery system for the different treatment protocols for diseases. For the tracheal stenosis case, it should be made to study the effect of the delayed separation in consequent generations to be able to observe how much it differs from the smooth models previously studied.

Finally, to test validate the accuracy from CFD RANS simulations we compared the second experiment with different RANS models simulations and we determined that traditional RANS algorithms, as they currently stand, are not reliable for research in respiratory fluid dynamics. It is therefore necessary to develop mathematical models that more accurately represent the flow within the airway. To develop these models, however, we need a better understanding of the flow physics, which requires high fidelity data from experiments or direct numerical simulations.

REFERENCES

Adler, K., & Brücker, C. (2007). Dynamic flow in a realistic model of the upper human lung airways. *Experiments in Fluids*, *43*(2–3), 411–423. https://doi.org/10.1007/s00348-007-0296-0

Adrian, R. J., & Westerweel, J. (2011). *Particle image velocimetry*. Cambridge University Press.

Bailly, C., & Comte-Bellot, G. (2015). Turbulence. In *The Journal of the American Academy of Psychoanalysis and Dynamic Psychiatry*. https://doi.org/10.1007/978-3-319-16160-0

Ball, C. G., Uddin, M., & Pollard, A. (2008). Mean flow structures inside the human upper airway. *Flow, Turbulence and Combustion*, *81*(1–2), 155–188. https://doi.org/10.1007/s10494-007-9113-3

Bauer, K., & Brücker, C. (2015). The influence of airway tree geometry and ventilation frequency on airflow distribution. *Journal of Biomechanical Engineering*, *137*(8), 81001. https://doi.org/10.1115/1.4030621

Bauer, K., Rudert, A., & Brücker, C. (2012). Three-Dimensional Flow Patterns in the Upper Human Airways. *Journal of Biomechanical Engineering*, *134*(7), 71006. https://doi.org/10.1115/1.4006983

Belka, M., Lippay, J., Lizal, F., Jedelsky, J., & Jicha, M. (2014). Comparison of methods for evaluation of aerosol deposition in the model of human lungs. *EPJ Web of Conferences*, *67*, 2006. https://doi.org/10.1051/epjconf/20146702006

Benjamin, B., Pitkin, J., & Cohen, D. (1981). Congenital tracheal stenosis. *The Annals of Otology, Rhinology, and Laryngology*, *90*(4 Pt 1), 364.

Bernate, J. A., Geisler, T. S., Padhy, S., Shaqfeh, E. S. G., & Iaccarino, G. (2017). *Study of the flow unsteadiness in the human airway using large eddy simulation*. *83101*, 1–18. https://doi.org/10.1103/PhysRevFluids.2.083101

Bocanegra Evans, H., & Castillo, L. (2016). Index-matched measurements of the effect of cartilaginous rings on tracheobronchial flow. *Journal of Biomechanics*, *49*(9), 1601–1606. https://doi.org/10.1016/j.jbiomech.2016.03.043

Breuer, M., Peller, N., Rapp, C., & Manhart, M. (2009). Flow over periodic hills - Numerical and experimental study in a wide range of Reynolds numbers. *Computers and Fluids*, *38*(2), 433–457. https://doi.org/10.1016/j.compfluid.2008.05.002

Brooke, J. W., Hanratty, T. J., & McLaughlin, J. B. (1994). Free-flight mixing and deposition of aerosols. *Physics of Fluids*, *6*(10), 3404–3415. https://doi.org/10.1063/1.868398

Brouns, M., Jayaraju, S. T., Lacor, C., Mey, J. De, Noppen, M., Vincken, W., … Verbanck, S. (2007). Tracheal stenosis: a flow dynamics study. *Journal of Applied Physiology*, *102*(3), 1178–1184. https://doi.org/10.1152/japplphysiol.01063.2006.

Chen, J., & Gutmark, E. (2014). Numerical investigation of airflow in an idealized human extra-thoracic airway: a comparison study. *Biomechanics and Modeling in Mechanobiology*, *13*, 205–214. https://doi.org/10.1007/s10237-013-0496-x

Choi, H., Jeon, W., & Kim, J. (2008). *Control of Flow Over a Bluff Body*. https://doi.org/10.1146/annurev.fluid.39.050905.110149

Coleman, G. N., Rumsey, C. L., & Spalart, P. R. (2018). Numerical study of turbulent separation bubbles with varying pressure gradient and Reynolds number. *Journal of Fluid Mechanics*, *847*, 28–70. https://doi.org/10.1017/jfm.2018.257

Comer, J. K., Kleinstreuer, C., & Zhang, Z. (2001a). Flow structures and particle deposition patterns in double-bifurcation airway models. Part 1. Air flow fields. *Journal of Fluid Mechanics*, *435*, 25–54.

Comer, J. K., Kleinstreuer, C., & Zhang, Z. (2001b). Flow structures and particle deposition patterns in double-bifurcation airway models. Part 2. Aerosol transport and deposition. *Journal of Fluid Mechanics*, *435*, 25–54.

Elcner, J., Lizal, F., Jedelsky, J., Jicha, M., & Chovancova, M. (2016). Numerical investigation of inspiratory airflow in a realistic model of the human tracheobronchial airways and a comparison with experimental results. *Biomechanics and Modeling in Mechanobiology*, *15*(2), 447–469. https://doi.org/10.1007/s10237-015-0701-1

Freitas, R. K., & Schröder, W. (2008). Numerical investigation of the three-dimensional flow in a human lung model. *Journal of Biomechanics*, *41*(11), 2446–2457. https://doi.org/10.1016/j.jbiomech.2008.05.016

Green, A. S. (2004). Modelling of peak-flow wall shear stress in major airways of the lung. *Journal of Biomechanics*, *37*(5), 661–667. https://doi.org/10.1016/j.jbiomech.2003.09.024

Grgic, B., Finlay, W., Heenan, A. (2004). Regional aerosol deposition and flow measurements in an idealized mouth and throat. *J. Aerosol*, *35*(1), 21–32.

Grobe, S., Schröder, W., Klaas, M., Klöckner, A., & Roggenkamp, J. (2007). Time resolved analysis of steady and oscillating flow in the upper human airways. *Experiments in Fluids*, *42*(6), 955–970. https://doi.org/10.1007/s00348-007-0318-y

Grotberg, J. B. (1994). Pulmonary Flow and Transport Phenomena. *Annual Review of Fluid Mechanics*, *26*(1), 529–571. https://doi.org/10.1146/annurev.fl.26.010194.002525

Gutmark, E. (2015). *Numerical investigation of airflow in an idealized human extra-thoracic airway: a comparison study*. *13*(1), 1–16. https://doi.org/10.1007/s10237-013-0496-x.Numerical

Hart, D. P. (1998). The Elimination of Correlation Errors in PIV Processing. *9th International Symposium of Applications of Laser Techniques to Fluid Mechanics, Lisbon, Portugal, 1998. Springer Verlag, 2000, i.*

Heenan, A. F., Matida, E., Pollard, A., & Finlay, W. H. (2003). Experimental measurements and computational modeling of the flow field in an idealized human oropharynx. *Experiments in Fluids*, *35*(1), 70–84. https://doi.org/10.1007/s00348-003-0636-7

Janke, T., Koullapis, P., Kassinos, S. C., & Bauer, K. (2019). PIV measurements of the SimInhale benchmark case. *European Journal of Pharmaceutical Sciences*, *133*(February), 183–189. https://doi.org/10.1016/j.ejps.2019.03.025

Janke, T., Schwarze, R., & Bauer, K. (2017). Measuring three-dimensional flow structures in the conductive airways using 3D-PTV. *Experiments in Fluids*, *58*(10), 133. https://doi.org/10.1007/s00348-017-2407-x

Johari, N. H., Osman, K., Basri, W. M., & Ngali, Z. (2012). Effect of tracheal stenosis at different locations on airflow in the trachea and main bronchi. *AIP Conference Proceedings*, *1440*(June), 1325–1332. https://doi.org/10.1063/1.4704355

Kim, S. K., & Chung, S. K. (2009). Investigation on the respiratory airflow in human airway by PIV. *Journal of Visualization*, *12*(3), 259–266. https://doi.org/10.1007/BF03181864

Kleinstreuer, C., & Zhang, Z. (2010). Airflow and Particle Transport in the Human Respiratory System. *Annual Review of Fluid Mechanics*, *42*(1), 301–334. https://doi.org/10.1146/annurev-fluid-121108-145453

Koullapis, P. G., Kassinos, S. C., Bivolarova, M. P., & Melikov, A. K. (2016). Particle deposition in a realistic geometry of the human conducting airways: Effects of inlet velocity profile, inhalation flowrate and electrostatic charge. *Journal of Biomechanics*, *49*(11), 2201–2212. https://doi.org/10.1016/j.jbiomech.2015.11.029

Koullapis, P., Kassinos, S. C., Muela, J., Perez-Segarra, C., Rigola, J., Lehmkuhl, O., … Nicolaou, L. (2018). Regional aerosol deposition in the human airways: The SimInhale benchmark case and a critical assessment of in silico methods. *European Journal of Pharmaceutical Sciences*, *113*(September 2017), 77–94. https://doi.org/10.1016/j.ejps.2017.09.003

Langtry, R. B., & Menter, F. R. (2009). Correlation-Based Transition Modeling for Unstructured Parallelized Computational Fluid Dynamics Codes. *AIAA Journal*, *47*(12), 2894–2906. https://doi.org/10.2514/1.42362

Li, Z., Kleinstreuer, C., & Zhang, Z. (2007). Particle deposition in the human tracheobronchial airways due to transient inspiratory flow patterns. *Journal of Aerosol Science*, *38*(6), 625–644. https://doi.org/10.1016/j.jaerosci.2007.03.010

Lin, C. L., Tawhai, M. H., McLennan, G., & Hoffman, E. A. (2007). Characteristics of the turbulent laryngeal jet and its effect on airflow in the human intra-thoracic airways. *Respiratory Physiology and Neurobiology*, *157*(2–3), 295–309. https://doi.org/10.1016/j.resp.2007.02.006

Lin, E., & Alessio, A. (2009). What are the basic concepts of temporal, contrast, and spatial resolution in cardiac CT? *Journal of Cardiovascular Computed Tomography*, *3*(6), 403–408. https://doi.org/10.1016/j.jcct.2009.07.003

Lizal, F., Jedelsky, J., Elcner, E., & Al., E. (2012). Research of Transport and Deposition of Aerosol in Human Airway Replica. *EPJ Web of Conferences*, *25*, 5–10. https://doi.org/10.1051/epjconf/2012250

Luo, H. Y., & Liu, Y. (2008). Modeling the bifurcating flow in a CT-scanned human lung airway. *Journal of Biomechanics*, *41*(12), 2681–2688. https://doi.org/10.1016/j.jbiomech.2008.06.018

Maas, H. G., Gruen, A., & Papantoniou, D. (1993). Particle tracking velocimetry in 3-dimensional flows. *Experiments in Fluids*, *15*(2), 133–146. https://doi.org/10.1007/BF00190953

Mauder, T., Jedelsky, J. and Lizal, F. (2009). Statistical Approach to Aerosol Transport Evaluation Under Cyclic Conditions. *Sborník Konference*, (1), 31–32. ÚT AV ČR.

Maury, B. (2013). *The Respiratory System in Equations*. Springer Science & Business Media.

Menter, F. R., Langtry, R., Völker, S., & Huang, P. G. (2005). Transition Modelling for General Purpose CFD Codes. *Engineering Turbulence Modelling and Experiments 6*, (August), 31–48. https://doi.org/10.1016/B978-008044544-1/50003-0

Minnich, D. J., & Mathisen, D. J. (2007). Anatomy of the trachea, carina, and bronchi. *Thoracic Surgery Clinics*, *17*(4), 571–585. https://doi.org/10.1016/j.thorsurg.2006.12.006

Montoya Segnini, J., Bocanegra Evans, H., & Castillo, L. (2018). Flow Recirculation in Cartilaginous Ring Cavities of Human Trachea Model. *Journal of Aerosol Medicine and Pulmonary Drug Delivery*, *31*(0), jamp.2017.1435. https://doi.org/10.1089/jamp.2017.1435

Munson, B. R., Young, D. F., & Okiishi., T. H. (1990). *Fundamentals of fluid mechanics* (4th ed.). New York: John Wiley & Sons.

Murgu, S., & Colt, H. (2013). Tracheobronchomalacia and Excessive Dynamic Airway Collapse. *Clinics in Chest Medicine*, *34*(3), 527–555. https://doi.org/10.1016/j.ccm.2017.11.015

Mylavarapu, G., Murugappan, S., Mihaescu, M., Kalra, M., Khosla, S., & Gutmark, E. (2009). Validation of computational fluid dynamics methodology used for human upper airway flow simulations. *Journal of Biomechanics*, *42*(10), 1553–1559. https://doi.org/10.1016/j.jbiomech.2009.03.035

Pedley, T. J., Schroter, R. C., & Sudlow, M. F. (2006). Flow and pressure drop in systems of repeatedly branching tubes. *Journal of Fluid Mechanics*, *46*(2), 365. https://doi.org/10.1017/S0022112071000594

Pope, S. B. (2001). Turbulent Flows. In *Cambridge University Press*. https://doi.org/10.1088/0957-0233/12/11/705

Raiesi, H., Piomelli, U., & Pollard, A. (2011). Evaluation of Turbulence Models Using Direct Numerical and Large-Eddy Simulation Data. *Journal of Fluids Engineering*, *133*(2), 21203. https://doi.org/10.1115/1.4003425

Ramuzat, A., & Riethmuller, M. L. (2002). PIV investigation of oscillating flows within a 3D lung multiple bifurcations model. *11th International Symposium Applications of Laser Techniques to Fluid Mechanics*, 8–11. Lisbon, Portugal.

Russo, J., Robinson, R., & Oldham, M. J. (2008). Effects of cartilage rings on airflow and particle deposition in the trachea and main bronchi. *Medical Engineering and Physics*, *30*(5), 581–589. https://doi.org/10.1016/j.medengphy.2007.06.010

Schroter, R. C., & Sudlow, M. F. (1969). Flow patterns in models of the human bronchial airways. *Respiration Physiology*, *7*(3), 341–355. https://doi.org/10.1016/0034-5687(69)90018-8

Schuurmans, M. M., & Bolliger, C. T. (2004). Silicone airway stents. *LUNG BIOLOGY IN HEALTH AND DISEASE*, *180*, 215–238.

Shuib, A. S., Hoskins, P. R., Easson, W. J., & Model, A. S. A. (2010). *Flow Regime Characterization in a Diseased Artery Model*. *4*(2), 87–91.

Song, S., Yang, X., Xin, F., & Lu, T. J. (2018). Modeling of surface roughness effects on Stokes flow in circular pipes. *Physics of Fluids*, *30*(2). https://doi.org/10.1063/1.5017876

Spittle, N., & McCluskey, A. (2000). Tracheal stenosis after intubation. *BMJ*, *321*(7267), 1000–1002. https://doi.org/10.1177/1479972316631139

Srivastav, V. K., Paul, A. R., & Jain, A. (2013). Effects of cartilaginous rings on airflow and particle transport through simplified and realistic models of human upper respiratory tracts. *Acta Mechanica Sinica/Lixue Xuebao*, *29*(6), 883–892. https://doi.org/10.1007/s10409-013-0086-2

Stapleton, K. W., Guentsch, E., Hoskinson, M. K., & Finlay, W. H. (2000). On the suitability of k-epsilon turbulence modeling for aerosol deposition in the mouth and throat: A comparison with experiment. *Journal of Aerosol Science*, *31*(6), 739–749. https://doi.org/10.1016/S0021-8502(99)00547-9

Taherian, S., Rahai, H., Gomez, B., Waddington, T., & Mazdisnian, F. (2017). Computational fluid dynamics evaluation of excessive dynamic airway collapse. *Clinical Biomechanics*, *50*(February), 145–153. https://doi.org/10.1016/j.clinbiomech.2017.10.018

Taherian, S., Rahai, H. R., Bonifacio, J., Gomez, B. Z., & Waddington, T. (2017). Particulate Deposition in a Patient With Tracheal Stenosis. *Journal of Engineering and Science in Medical Diagnostics and Therapy*, *1*(1), 11005. https://doi.org/10.1115/1.4038260

Tropea, C., Yarin, A. L., & Foss, J. F. (2007). *Springer Handbook of Experimental Fluid Mechanics* (Vol. 1). Springer Science & Business Media.

Weibel, E. R. (1963). Geometry and Dimensions of Airways of Conductive and Transitory Zones. In *Morphometry of the Human Lung*. (pp. 110–135). Springer Berlin Heidelberg.

Zhang, Y., & Finlay, W. H. (2005). Measurement of the Effect of Cartilaginous Rings on Particle Deposition in a Proximal Lung Bifurcation Model. *Aerosol Science and Technology*, *39*(5), 394–399. https://doi.org/10.1080/027868290945785

Zhang, Z., Kleinstreuer, C., & Kim, C. S. (2002). Aerosol deposition efficiencies and upstream release positions for different inhalation modes in an upper bronchial airway model. *Aerosol Science and Technology*, *36*(7), 828–844. https://doi.org/10.1080/02786820290092078

Zhao, Y., & Lieber, A. (1994). Steady Inspiratory Flow in a Model Symmetric Bifurcation. *Journal of Biomechanical Engineering*, *116*(4), 488–496.